

GPS Research

Christos Vasileios Kokas

27-1-2021

Contents

1 GPS	6
1.1 How GPS Works	6
2 RTK GPS	7
2.1 Base-Rover RTK GPS	7
2.1.1 Base-Rover RTK Receivers	7
2.1.2 Corrections over NTRIP	8
2.1.3 How Base-Rover RTK GPS Works	9
2.2 GNSS/INS RTK GPS	10
2.2.1 How GNSS/INS RTK GPS Works	10
2.2.2 GNSS/INS vs Base-Rover	10
2.3 Products and Companies	11
2.3.1 Ellipse-D (SBG Systems)	11
2.3.2 AsteRx SBi3 Pro+ (Septentrio)	15
2.3.3 MTi-680G (XSENS)	16
2.3.4 X1 (BYNAV)	18
2.3.5 μ INS (Inertial Sense)	20
2.3.6 3DMGQ7-GNSS/INS (Parker Lord)	21
2.4 Prices	22
3 Solid State LiDAR	23
3.1 LiDAR versus Solid State LiDAR	23
3.2 How Solid State LiDAR Works	24
3.3 % Reflectivity	25
3.4 Products and Companies	25
3.4.1 Velarray H800 (Velodyne)	25
3.4.2 Velarray M1600 (Velodyne)	26
3.4.3 Velabit (Velodyne)	27
3.4.4 RS-LiDAR-M1 (Robosense)	29
3.4.5 S3-2 (Quanergy)	30
3.4.6 Cube 1 (Blickfeld)	32
3.4.7 Cube Range 1 (Blickfeld)	34
3.4.8 L515 (INTEL)	35
3.4.9 4Sight M (AEYE)	37
3.4.10 OS0,OS1,OS2 (Ouster)	38
3.4.11 HPS-3D160 Pro, HPS-3D640 (Hypersen)	40

3.4.12	Leddar Pixell (LeddarTech)	42
3.4.13	AVIA (LIVOX)	44
3.4.14	CE30 (Benewake)	44
3.4.15	Aeries (AEVA)	45
3.4.16	Iris (Luminar)	47
3.4.17	Sora-P Family (Cepton)	47
3.4.18	Vista-X Family (Cepton)	49
3.4.19	Nova (Cepton)	50
3.4.20	QT128 (Hesai)	52
3.4.21	AT128 (Hesai)	53
3.4.22	Pandar128 (Hesai)	54
3.4.23	XT32 (Hesai)	56
3.4.24	POWER-W (Genius-Pros)	57
3.4.25	POWER-PBA2 (Genius-Pros)	58
3.4.26	ULTRA-UGC1 (Genius-Pros)	59
3.4.27	ULTRA-UGC2 (Genius-Pros)	59
3.4.28	TetraVue 4D Flash LiDAR (tetravue)	60
3.4.29	AX32 (ABAX SENSING)	61
3.4.30	OPAL-3 Conical/Panoramic (NeptecThechnologies)	62
3.4.31	InnovizOne (Innoviz Technologies)	63
3.4.32	InnovizTwo (Innoviz Technologies)	64
3.4.33	Innoviz360 (Innoviz Technologies)	65
3.4.34	InnovizPro (Innoviz Technologies)	66
3.4.35	Lumotive M30 (Lumotive)	66
3.4.36	Lumotive U30 (Lumotive)	67
3.4.37	Lumotive L30 (Lumotive)	68
3.4.38	ML (SosLab)	68
3.4.39	XenoLidar Xact (Xenomatix)	69
3.4.40	XenoLidar Xpert (Xenomatix)	70
3.4.41	SP2.5/SP3.0 (Opsys)	70
3.4.42	Spectrum HD (Baraja)	71
3.4.43	Spectrum Off-Road (Baraja)	71
3.4.44	ibeoNEXT (Ibeoautomotive)	72
3.4.45	ibeo LUX (Ibeoautomotive)	72
3.4.46	Dynamic View LiDAR or A-Sample (Microvision)	75
3.5	Differences	75

4 LiDAR Introduction	79
4.1 Types of LiDARs	81
4.2 LiDAR Detection Modes	82
4.3 Monostatic versus Bistatic LiDAR	83
4.4 Transmit/Receive Isolation	83
5 LiDAR Range Equation	84
5.1 Illuminator Beam	84
5.2 LiDAR Cross-Section	86
5.3 Power Calculation	87
5.4 Atmospheric Losses	87
5.5 Atmospheric Turbulence	87
5.6 Speckle	88
6 Types of LiDAR	89
6.1 Direct-Detection LiDAR	89
6.1.1 1D Range-Only LiDAR	89
6.1.2 Tomographic Imaging LiDAR	89
6.1.3 Range-Gated Active Imaging (2D LiDAR)	90
6.1.4 3D Scanning LiDAR	90
6.1.5 3D Flash Imaging	91
6.1.6 3D Mapping Applications	91
6.1.7 Laser Vibration Detection	92
7 LiDAR Sources	92
7.1 Laser Waveforms	93
7.1.1 High Time-Bandwidth Product Waveforms	95
7.1.2 Polypulse Waveform	95
7.1.3 Linear Frequency Modulation	95
7.1.4 Q-Switched Lasers for LiDAR	96
7.1.5 Diode Lasers of LiDARs	96
8 LiDAR Receivers	97
8.1 Introduction	97
8.2 LiDAR Signal-to-Noise Ratio	98
8.3 Noise Probability Density Functions	99
8.3.1 Thermal Noise	99
8.3.2 Shot Noise	100

8.3.3	Background Noise	101
8.3.4	Dark Current Noise	101
8.3.5	Avalanche Photodiodes	102
9	LiDAR	104
9.1	Coherent LiDAR	104
10	Lane Detection	104
11	Visual Odometry (VO)	104
11.1	Feature-Based Approach	105
12	Ideas	105

1 GPS

The Global Positioning System (GPS) is a navigation system using satellites, a receiver and algorithms to synchronize location, velocity and time data for air, sea and land travel. While only three satellites are needed to produce a location on earth's surface, a fourth satellite is often used to validate the information from the other three. The fourth satellite provides the ability to calculate the altitude of a device. GPS is made up of three different components, called segments, that work together to provide location information. The three segments of GPS are:

- Space (Satellites) — The satellites circling the Earth, transmitting signals to users on geographical position and time of day.
- Ground control — The Control Segment is made up of Earth-based monitor stations, master control stations and ground antenna. Control activities include tracking and operating the satellites in space and monitoring transmissions.
- User equipment — GPS receivers and transmitters including items like watches, smartphones and telematic devices.

1.1 How GPS Works

GPS works through a technique called trilateration. Trilateration is a mathematical technique used by a GPS device to determine user position, speed, and elevation. By constantly receiving and analyzing radio signals from multiple GPS satellites and applying the geometry of circles, spheres, and triangles, a GPS device can calculate the precise distance or range to each satellite being tracked. Trilateration is a sophisticated version of triangulation, though it does not use the measurement of angles in its calculations. Data from a single satellite provides a general location of a point within a large circular area on the Earth's surface. Adding data from a second satellite allows the GPS to narrow the specific location of that point down to a region where the two areas of satellite data overlap. Adding data from a third satellite provides an accurate position of the point on the Earth's surface.

All the GPS devices require three satellites for an accurate calculation of position. Data from a fourth satellite—or even more than four satellites—further enhance the precision of the point's location, and also allows

factors such as elevation or, in the case of aircraft, altitude to also be calculated.

2 RTK GPS

Real-time kinematic positioning (RTK) is the application of surveying to correct for common errors in current satellite navigation (GNSS (GNSS receivers measure how long it takes for a signal to travel from a satellite to the receiver)) systems. It uses measurements of the phase of the signal's carrier wave in addition to the information content of the signal and relies on a single reference station or interpolated virtual station to provide real-time corrections, providing up to centimetre-level accuracy [1].

2.1 Base-Rover RTK GPS

2.1.1 Base-Rover RTK Receivers

Two receivers are used in RTK. One of them is stationary, another moves freely. They are called base station and rover as presented in Figure 2.1.

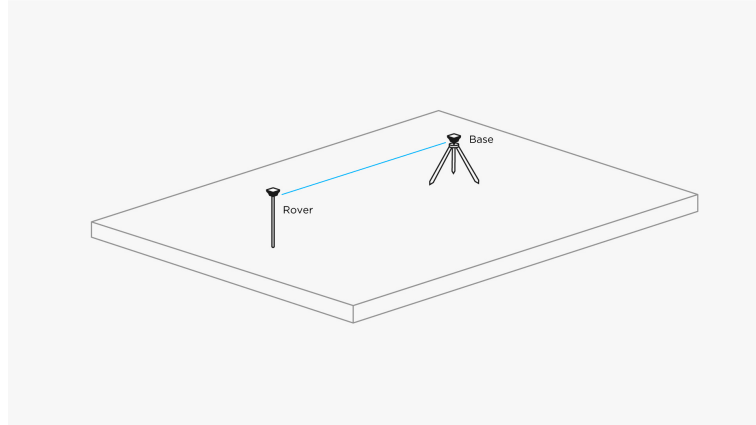


Figure 2.1: RTK Base and Rover

The base stays in one place and sends corrections to a moving receiver. The receiver uses that data to achieve centimeter precise position. Any number of receivers can connect to one base if their input settings match the base's output, as presented in Figure 2.2.

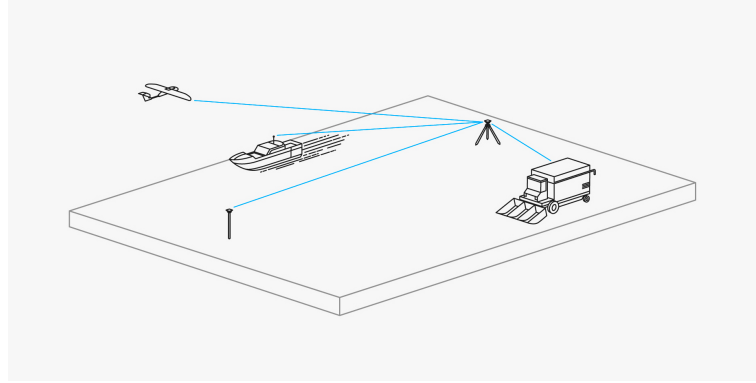


Figure 2.2: RTK Base and Multiple Receivers

2.1.2 Corrections over NTRIP

The base can also share corrections over the Internet. This technology is called NTRIP (Networked Transport of RTCM via Internet Protocol) which enables the mobile RTK GPS receiver (rover) to access data from the RTK base station over the internet. Some of the benefits of using NTRIP are :

- Less equipment to carry in the field. Almost all data collectors, smartphones, and computers have the capability to connect to the internet even in a field setting.
- Mitigate the chance of radio interference.
- No limitation on communication range.

One limitation of NTRIP is :

- it requires the work area to be in range of cellular service for receiving corrections data via the Internet.

NTRIP consists of two pieces of software which communicate over the internet. The server side runs NTRIP Caster software. The rover side runs the NTRIP Client software. The NTRIP caster is responsible for receiving the data stream from the base receiver and rebroadcasting it over a specified TCP (Transmission Control Protocol) port.

An example of how NTRIP works is presented in Figure 2.3.

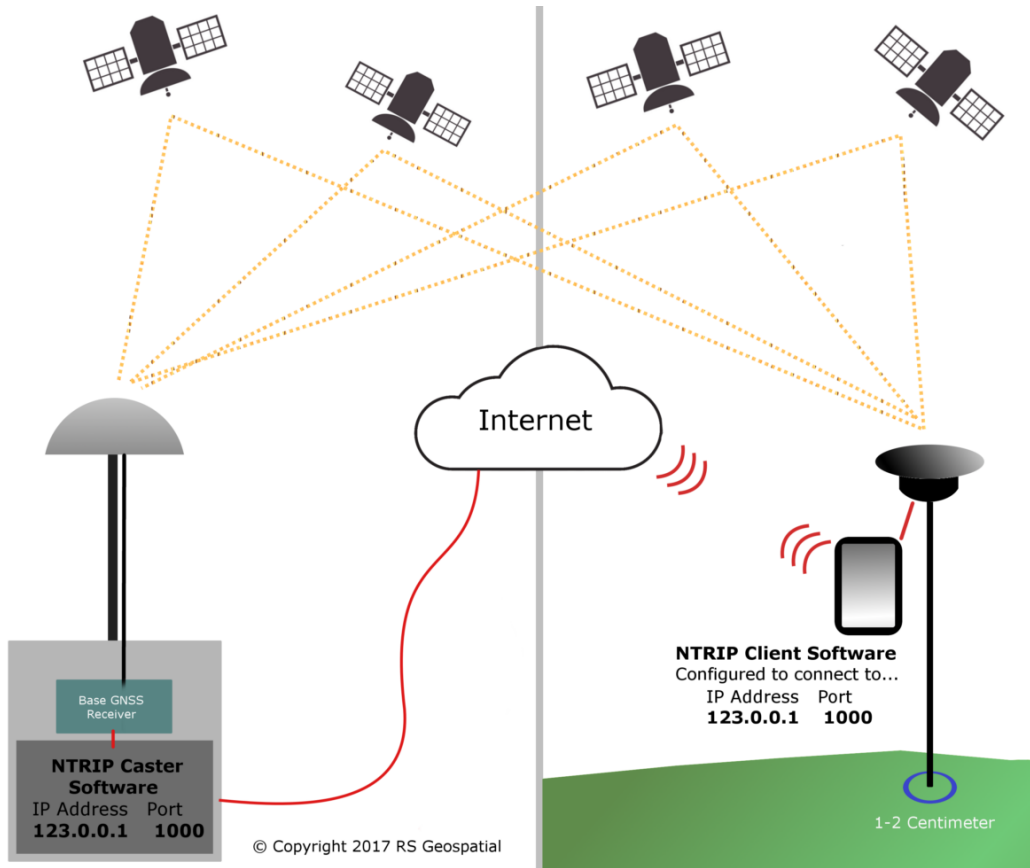


Figure 2.3: How NTRIP Works

2.1.3 How Base-Rover RTK GPS Works

Base-Rover RTK works by having the RTK base station set up at a known geospatial location. The RTK base station receiver is set to the known latitude/longitude/height of this point during setup. The base receiver continuously observes the satellites and calculates position corrections that are sent to the mobile receiver (rover) with a set frequency (most usual frequency is once every second) in a data stream. The rover uses location information from the satellites (GNSS) and the base correctional data to compute a precise coordinate.

2.2 GNSS/INS RTK GPS

The Global Navigation Satellite System (GNSS) is a satellite configuration, or constellation, that provides satellite signals to a GNSS receiver which can be used to calculate position, velocity, and time. An inertial navigation system (INS) uses an inertial measurement unit (IMU) consisting of micro-electromechanical system (MEMS) inertial sensors to measure the system's angular rate and acceleration. Measurements from each of these two systems can be combined using advanced Kalman filtering estimation techniques to form a GNSS-aided INS system (GNSS/INS). This combined system is able to provide position, velocity, and attitude estimates of higher accuracies and with better dynamic performance than a standalone GNSS or INS system can provide.

2.2.1 How GNSS/INS RTK GPS Works

Both the INS and GNSS can track the position and velocity of the system. An INS typically has reduced errors in the short-term, but larger, unbounded errors over extended periods of time. In contrast, GNSS tends to be noisier in the short-term, but can provide more stability over longer periods of time. When the two systems are integrated together, the GNSS measurements are able to regulate the INS errors and prevent their unbounded growth. On the other hand, an INS can provide a navigation solution at high output rates, while a GNSS navigation solution is typically only updated at rates between 1 Hz and 10 Hz. Combining the measurements from these two systems allows the INS solution to bridge the gap between GNSS updates. A GNSS/INS system uses a Kalman filter to track an optimal estimate of the system's position, velocity, attitude, gyro bias, and accelerometer bias.

2.2.2 GNSS/INS vs Base-Rover

In contrast to the base-rover RTK GPS that needs a base to provide cm-level accuracy, by combining GNSS with INS the same cm-level accuracy can be achieved without the requirement of having a base providing error correction. In Paragraph 2.3 products that utilize GNSS/INS RTK GPS are presented.

2.3 Products and Companies

2.3.1 Ellipse-D (SBG Systems)

Ellipse-D, manufactured by SBG Systems, is the smallest Inertial Navigation System integrating a Dual-antenna, multi-band GNSS receiver, capable of delivering precise heading as well as centimeter level position accuracy in the most challenging GNSS conditions [2]. The product line for the Ellipse Series are presented in Figure 2.4.

				
	Ellipse-A	Ellipse-E	Ellipse-N	Ellipse-D
Application	Motion Sensor	INS with your own GNSS receiver	INS for dynamic and automotive applications	INS for low dynamics and robust heading
Heading	Magnetic	Magnetic or GNSS	Magnetic or Mono-antenna GNSS	Dual antenna GNSS
Heave: 5 cm or 5%	•	•	•	•
Odometer aiding		Pulse / CAN OBD-II	Pulse / CAN OBD-II	Pulse / CAN OBD-II
Navigation		Navigation with external GNSS receiver	L1/L2 GNSS receiver 1cm RTK GNSS Accuracy	L1/L2 GNSS receiver 1cm RTK GNSS Accuracy
Post-Processing	•	•	•	•

Figure 2.4: Ellipse Series Product Line

The mechanical properties of the each product in the product line are presented in Figure 2.5.

MECHANICAL

Box version are IP68, resistant to dust and water.
OEM version are PCB mounted for tight integration.

Model	A	E	N	D
Box				
Size	46 x 45 x 24 mm	46 x 45 x 24 mm	46 x 45 x 24 mm	46 x 45 x 32 mm
Weight	45 g	47 g	49 g	65 g
OEM				
Size	29.5 x 25.5 x 11 mm	29.5 x 25.5 x 11 mm	29.5 x 25.5 x 16 mm	29.5 x 25.5 x 16 mm
Weight	8 g	8 g	17 g	17 g

Figure 2.5: Mechanical Properties of the Product Line

The accuracy and the interfaces are presented in Figure 2.6.

ACCURACY (RMS) 360° sensing in all axes, no mounting limitation

Model	A	E ⁽¹⁾ / N / D
Roll / Pitch	0.1°	0.1° SP 0.05° RTK 0.03° PPK ⁽⁴⁾
Heading	0.8° Magnetic ⁽²⁾	0.2° Dual antenna 2m 0.2° Single antenna with dynamics 0.1° PPK ⁽⁴⁾
Velocity⁽³⁾	-	0.03 m/s
Navigation⁽³⁾	-	1.2 m Single Point 1 m SBAS 1 cm RTK / PPK ⁽³⁾ + 1 ppm
Heave accuracy	5 cm or 5% - Valid for Marine version	
Heave period	Up to 15 s - Automatically adjusts to the wave period	

⁽¹⁾ With Supported GNSS receiver

⁽²⁾ Under homogenous magnetic field

⁽³⁾ Under good GNSS availability

⁽⁴⁾ Optional PPK = Post-processing Kinematic

INTERFACES

Available data	Euler angles, quaternion, velocity, position, heave, calibrated sensor data, delta angles & velocity, barometric data, status, GPS data, UTC time, GNSS raw data (Post-processing), etc.
Aiding sensors	GNSS, Odometer, RTCM
Output rate	200 Hz, 1,000 Hz (IMU data)
Main Serial Interface	RS-232, RS-422, USB - up to 921,600 bps
Serial protocols	Binary eCom, NMEA, ASCII, TSS
CAN interface	CAN 2.0A/B - up to 1 Mbit/s
Pulses	Inputs: Events, PPS, DMI (Direction or quadrature) Outputs: Synchronization (PPS) Model A/N/D: 2 inputs / 1 output Model E: 4 inputs / 2 outputs

Figure 2.6: Accuracy and Interfaces

The sensor properties are presented in Figures 2.7-2.8.

SENSORS

	Accelerometers	Gyroscopes	Magnetometers
Gain stability	1000 ppm	500 ppm	< 0.5 %
Non-linearity	1500 ppm	50 ppm	< 0.1 % FS
Bias stability	± 5 mg	± 0.2 °/s	± 1 mGauss
Random walk Noise density	57 µg/√Hz	0.15 °/√hr	3 mGauss
Bias in-run instability⁽¹⁾	14 µg	7 °/h	1.5 mGauss
VRE	50 µg/g ² RMS	1 °/h/g ² RMS	-
Alignment error	< 0.05 °	< 0.05 °	< 0.1 °
Bandwidth	390 Hz	133 Hz	22 Hz

⁽¹⁾ Allan Variance, @ 25 °C

Figure 2.7: Sensor Properties

PRESSURE SENSOR (models E/N/D)

Resolution	1.2 Pa / 10 cm / 0.3 ft
Pressure accuracy	± 50 Pa / ± 200 Pa Relative / Absolute

Figure 2.8: Pressure Sensor Properties

The electrical and environmental properties are presented in Figure 2.9.

ELECTRICAL & ENVIRONMENTAL

Input voltage	5 - 36 V
Power consumption	A/E: < 300 mW N ⁽¹⁾ : < 600 mW D ⁽¹⁾ : < 900 mW
Specified temperature	-40 to 85 °C
Shock limit	2,000 g
Operating vibration	8 g RMS (20 Hz to 2 k Hz per MIL-STD 810G)
MTBF	50,000 hours

⁽¹⁾ Without GNSS antenna

Figure 2.9: Electrical and Environmental Properties

2.3.2 AsteRx SBi3 Pro+ (Septentrio)

AsteRx SBi3 Pro+ GNSS/INS multi-frequency receiver delivers reliable centimeter level positioning together with 3D orientation in challenging environments. Thanks to the built-in inertial sensor, it provides orientation (heading, pitch and roll) as well as dead reckoning, making it ideal for systems that require positioning under any condition. This housed high-performance GNSS/INS system is ideal for rapid integration into machine control or ground robotic applications. AsteRx SBi3 Pro+ is the most flexible boxed GNSS/INS solution, offering full access to raw GNSS and INS data as well as allowing multiple antenna configurations [3].

AsteRx SBi3 Pro+ is presented in Figure 2.10.



Figure 2.10: AsteRx SBi3 Pro+

2.3.3 MTi-680G (XSENS)

The MTi-680G represents the highest standard in GNSS/INS (Global Navigation Satellite System/Inertial Navigation System) with an internal, integrated Real-Time Kinematic receiver (RTK). With the MTi-680G's added RTK feature, you can improve your positional data from meter-level to centimeter-level accuracy. You also benefit from sub 0.5 degree orientation estimates, and a rugged, IP68-rated housing at an industry-breaking price point. You can seamlessly integrate the MTi-680G in your application and it is highly flexible, with native CAN support. The MTi-680G RTK GNSS/INS comes as an industrial-grade, highly affordable MEMS-based orientation sensor with an integrated sensor fusion algorithm and an easy-to-use Starter Kit [4].

Mti-680G's technical specifications are presented in Figures 2.11-2.12.

Sensor fusion performance	Sensing Components
<ul style="list-style-type: none"> • Roll, Pitch 0.2 deg RMS • Yaw/Heading 0.8 deg RMS • Position 1cm CEP • Velocity 0.05m/s RMS 	<ul style="list-style-type: none"> • Gyroscope Standard full range: 2000 deg/s In-run bias stability: 8 deg/h Noise density: 0.007 °/s/$\sqrt{\text{Hz}}$ • Accelerometer Standard full range: 10g In-run bias stability: 10 (x,y) 15(z) μg Noise density: 60 $\mu\text{g}/\sqrt{\text{Hz}}$ • Magnetometer Available • GNSS receiver Brand: u-blox Model: ZED F9 • Barometer Available

Figure 2.11: Mti-680G's Sensor fusion Performance and Sensing Components

System Specifications
<ul style="list-style-type: none"> • Mechanical IP-rating (equivalent): IP68 Dimensions: 28x31.50x13 mm Weight: 8.9 gram
<ul style="list-style-type: none"> • Electrical Input voltage: 4.5 to 24V Power consumption (typ.): <1 W
<ul style="list-style-type: none"> • Interfaces / IO Interfaces: UART, CAN, RS232 Protocols: Xbus, ASCII (NMEA) or CAN Output frequency: 1kHz, 400Hz SDI

Figure 2.12: Mti-680G's System Specifications

Mti-680G is presented in Figure 2.13.



Figure 2.13: Mti-680G

2.3.4 X1 (BYNAV)

X1 optimally combines high-accuracy, low bandwidth GNSS measurements with high bandwidth IMU measurements to provide high-accuracy, low latency position, velocity, and attitude measurements, providing reliable and accurate centimeter-level position, velocity, acceleration and 3D orientation information under the most demanding environments [5].

In Figure 2.14 the specifications of BYNAV's X1 are presented.

System Type		GNSS/INS Integrated System	
Physical Properties		Dimensions Weight Typical Power Consumption	116mm×114.2mm×38.6mm 432g 4.8W
Signal Frequency		BDS BDS-3 GPS GLONASS QZSS Galileo	B1, B2 B1C, B2a L1, L2 G1, G2 L1, L2 E1, E5b
Com Port Number		Serial Port CAN Port Ethernet Port 1PPS	2 1 1 1
Performance		Accuracy in GNSS Signal Loss RTK Horizontal Accuracy DGPS Horizontal Accuracy Timing Accuracy Orientation Accuracy Velocity Measurement Accuracy RTK + Orientation Solution Frequency Raw Data Output	10s 0.3m 1.0cm + 1ppm RMS 0.5m + 1ppm RMS 20ns RMS 0.20°/m RMS 0.05m/s RMS Supports 200Hz Default 100Hz Support

Figure 2.14: X1 Specifications

The X1 GNSS/INS Receiver is presented in Figure 2.15.



Figure 2.15: X1 GNSS/INS Receiver

2.3.5 μ INS (Inertial Sense)

The Inertial Sense μ INS is a miniature, GPS (GNSS) aided Inertial Navigation System (GPS-INS) module that includes all functionality of the μ AHRS and provides orientation, velocity, and position. Base station corrections data can be applied to achieve CM level precision.

Sensor data from MEMS gyros, accelerometers, magnetometers, barometric pressure, and GPS/GNSS is fused to provide optimal estimation.

Data out includes angular rate, linear acceleration, magnetic field, barometric altitude, and GPS time [6].

μ INS's key features are :

- 0.1° roll and pitch
- 0.3° GPS heading
- 3cm RTK position accuracy
- Up to 1000Hz output rate
- Onboard World Magnetic and Gravity Models
- Strobe In/Out Data Sync
- Attitude (Quaternions, Euler, DCM)

μ INS is presented in Figure 2.16.



Figure 2.16: μ INS

2.3.6 3DMGQ7-GNSS/INS (Parker Lord)

The 3DMGQ7 GNSS/INS is an all-in-one navigation solution featuring centimeter-level position accuracy. It features dual-antenna, RTK enabled INS designed for outstanding performance, even in unpredictable conditions. It is equipped with dual multiband GNSS receivers, low noise and low drift MEMS inertial sensors, and a robust adaptive Kalman filter [7]. The 3DMGQ7 GNSS/INS specifications are presented in Figure 2.17.

Sensor	Operation	Package
<ul style="list-style-type: none"> Up to 1 cm + 1 ppm positional accuracy with RTK Multi-frequency GNSS receivers provide 1.2m single point L1/L2 position accuracy Multi-constellation receivers with 184 tracking channels each allow for rapid signal acquisition and robust signal tracking in challenging GNSS environments Dual GNSS antenna heading with 0.2° heading accuracy that is immune to magnetic disturbances Tactical grade IMU with <2°/hr bias instability provides exceptional position accuracy during GNSS outages 0.1° pitch/roll accuracy 	<ul style="list-style-type: none"> Accepts standard RTCM real-time kinematic (RTK) corrections Adjustable sampling rates up to 1KHz 34 state auto-adaptive EKF Independently configurable IMU, GNSS, EKF outputs Forward compatible MIP Protocol optimizes bandwidth SensorConnect software for configuration, control, display, and logging MSCL open source API for easy integration 	<ul style="list-style-type: none"> Anodized Aluminum Precision alignment features Highly compact and low profile <ul style="list-style-type: none"> 76 mm x 68.6 mm x 13.3 mm 78 grams USB and RS-232 interfaces -40 to +85°C operating temperature range

Figure 2.17: 3DMGQ7 GNSS/INS Specifications

The 3DMGQ7 GNSS/INS is presented in Figure 2.18.



Figure 2.18: 3DMGQ7 GNSS/INS

2.4 Prices

The prices were found on the Internet, so they may differ.

Model	Price
Ellipse-D	Unknown
AsteRx SBi3 Pro+	Unknown
MTi-680G	\$3,100.00
X1	\$3,000.00
μ INS	\$2,500.00
3DMGQ7-GNSS/INS	Unknown

Table 1: Prices

3 Solid State LiDAR

3.1 LiDAR versus Solid State LiDAR

Traditional LiDAR systems are electromechanical—they rely on moving parts that have to be precise and accurate in order to obtain measurements suitable for autonomous navigation. These measurements come from photons from a laser, which then reflect back off surfaces and concentrate into a collector that can determine the distances of these objects. The laser and collector must rotate in order to scan the area around it. The moving parts involved put a restriction on the size of the system, since making them small and compact would increase the difficulties in the precise manufacturing required, which then drives up cost. Additionally, moving parts mean that it could be susceptible to perturbations, so driving in rough terrain for example could have negative impacts on readings. Solid-state LiDAR on the other hand is a system built entirely on a silicon chip. No moving parts are involved, which not only makes more resilient to vibrations, but can be made smaller much more easily. This lends to production being cheaper.

3.2 How Solid State LiDAR Works

In order to achieve a scan, solid-state LiDAR uses a concept not unlike phased array in radio. In phased array, several transmitters emit in certain patterns and phases to create a directional broadcast. The size, focus, and direction of this broadcast can be changed, without having to physically adjust the transmitters. The very same concept is applied in solid-state LiDAR to achieve optical phased array: optical emitters send out bursts of photons in specific patterns and phases to create directional emission, of which the focus and size can be adjusted. Once again, no physical adjustment to the optical emitters need to be made to achieve this, making it resilient to vibrations and more compact. How the solid-state LiDAR works and what it detects are presented in Figure 3.1 and Figure 3.2 respectively. A Video explaining the process can be found [here](#).

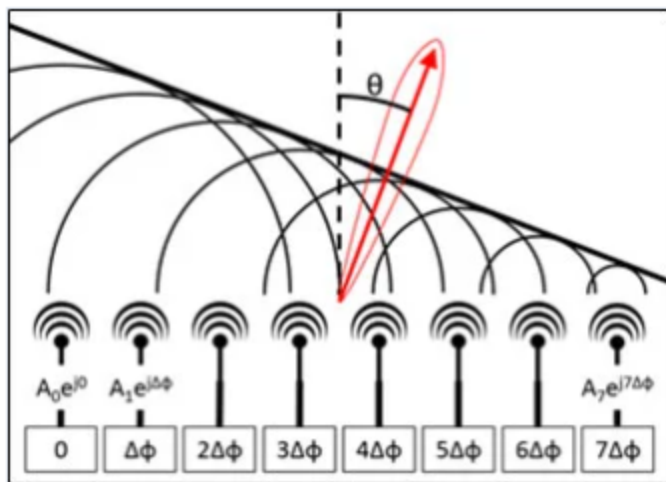


Figure 3.1: How Solid State LiDAR Works

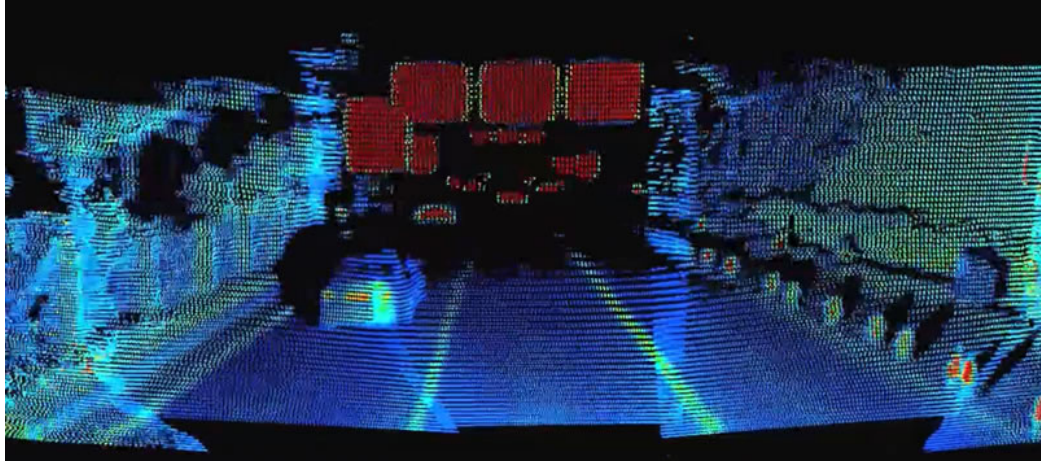


Figure 3.2: Solid State LiDAR Detection

3.3 % Reflectivity

The range of a Solid-State LiDAR depends on the % reflectivity of the target. The % reflectivity means that the target reflects % of the light that reaches the target. Having a high range LiDAR at targets with low reflectivity is better than having a high range LiDAR at targets with high reflectivity. Reflectivity is important because as mentioned in Section 3.2, solid-state LiDARs function using photons so reflectivity of the target is needed for a satisfactory result.

3.4 Products and Companies

3.4.1 Velarray H800 (Velodyne)

With the Velarray H800, Velodyne delivers the optimal solid state lidar sensor for advanced driver assistance systems (ADAS) and autonomous applications. The H800's long-range combined with a wide horizontal field of view (FOV) detects objects early enough to enable safe stopping distances in urban driving scenarios and collision avoidance on curves and turns [8].

Velarray H800's key features are :

- Solid state lidar
- Perception data at a range of 0.1 m to 200 m supporting safe stopping distances at highway speeds

- Configurable frame rate and resolution
- Advances driver assistance features including Automatic Emergency Braking and Lane Keeping Assist
- Compact, embeddable form factor for seamless interior/exterior integration
- Specifically designed for automotive grade performance
- Built using Velodyne's breakthrough micro-lidar array (MLA) architecture, a robust and reliable design for mass production

The Velarray H800 is presented in Figure 3.3.



Figure 3.3: Velarray H800

3.4.2 Velarray M1600 (Velodyne)

Designed for autonomous applications in sidewalk, commercial and industrial settings, the Velarray M1600 provides outstanding near-field perception for safe navigation in diverse environmental conditions [9].

Velarray M1600's key features are :

- Solid state lidar
- Enables touchless mobile and last-mile delivery robots to operate autonomously and safely, without human intervention

- Perception data at a range from 0.1 to 30 meters and a broad 32-degree vertical field of view, supporting smooth operation in crowded areas
- Ideal for sidewalks, commercial and industrial settings
- Compact, embeddable form factor for seamless interior/exterior integration
- Indoor/outdoor and day/night performance
- Configurable frame rate and resolution
- Built using Velodyne's breakthrough micro-lidar array (MLA) architecture, a robust and reliable design for mass production

The Velarray M1600 is presented in Figure 3.4.



Figure 3.4: Velarray M1600

3.4.3 Velabit (Velodyne)

The next generation Velabit, Velodyne's smallest sensor, brings new levels of versatility and affordability to 3D lidar perception. This compact, mid-range lidar sensor now offers a dramatic improvement in field of view: 90 degrees horizontal by 70 degrees vertical. It is highly configurable for specialized use cases and can be embedded almost anywhere within vehicles, robots, UAVs, infrastructure, and more. With the Velabit™, the possibilities are endless [10].

- Expanded, simultaneously achievable horizontal (90°) and vertical (70°) field of view
- Delivers high-resolution for customer perception needs with configurable and dynamic field of view
- Small form factor for sleek, embeddable design: lightweight (125g) and compact (2.4” x 2.4” x 1.38”) with integrated processing for a wide range of solutions
- Range of up to 100 meters
- Low power consumption (3-6W) maximizes battery life and vehicle range
- Proven Class 1 eye-safe 903 nanometer technology
- Bottom connector with cable length options
- Built to easily scale: multiple manufacturing sources available for qualified production projects

The Velabit Solid State LiDAR is presented in Figure 3.5.



Figure 3.5: Velabit

All of Velodyne's LiDARs are controlled through the Vella Development Kit (VDK). Vella Development Kit (VDK) provides access to Velodyne Lidar's breakthrough lidar-based perception software, paired with Velodyne's world-class sensors. VDK allows to plug in Velodyne's lidar with an off-the-shelf library of functions.

3.4.4 RS-LiDAR-M1 (Robosense)

RS-LiDAR-M1 is an automotive grade solid-state LiDAR, that RoboSense specially designed for massive production vehicles. It provides highly reliable 3D environment perception for vehicles to deliver safe driving [11].

The RS-LiDAR-M1 and its specifications are presented in Figure 3.8 and Figure 3.7 respectively.



Figure 3.6: RS-LiDAR-M1

Laser Wavelength	905nm	Laser Safety	Class 1 eye safe
Range	200m(150m@10% NIST)	Blind Spot	$\leq 0.5m$
Accuracy(Typical)	$\pm 5\text{cm}(1\sigma)$	Frame Rate	10~20Hz(Adjustable)
Horizontal FoV	120°(-60°~+60°)	Vertical FoV	25°(-12.5°~+12.5°)
Horizontal Resolution	0.2°(Average)	Vertical Resolution	0.2°(Average)
Points Per Second	~750,000pts/s(Single Return) ~1,500,000pts/s(Dual Return)	UDP Packet include	Spatial Coordinates, Intensity, Timestamp, etc.
Ethernet Connection	1000M Base T1	Output	UDP packets over Ethernet
Operating Voltage	9V - 36V	Operating Temperature	-40°C ~ +85°C
Power Consumption	15W	Storage Temperature	-40°C ~ +105°C
Ingress Protection	IP67, IP6K9K	Time Synchronization	gPTP
Dimension(Without connector)	108mm x 110mm x 45mm (D x W x H)	Weight (without cabling)	~730g

Figure 3.7: RS-LiDAR-M1 Specifications

3.4.5 S3-2 (Quanergy)

Quanergy's S3 solid state family of LiDAR sensors contains no moving or vibrating parts on either macro or micro scales. This enables the highest level of performance, longevity and cost efficiency with increasingly smaller footprints that require less power. The high reliability characteristic of the S3 family is especially important in environments where equipment up-time is essential for efficiency and profitability. In addition, the compact package enables seamless integration for smart, capable, always-aware perceptive vision [12].

Quanergy's S3-2 is presented in Figure 3.8.



Figure 3.8: S3-2

There are 3 different S3-2 models :

- S3-2NSI-S00
- S3-2NSO-S00
- S3-2WSO-S00

Their differences are presented in Figure 3.9.

SPECIFICATIONS	S3-2NSI-S00	S3-2NSO-S00	S3-2WSO-S00
Laser Class	Class 1 Laser Product (eye safe IEC 60825-1)		
Wavelength	905nm		
Measurement Technique	Time of Flight (TOF)		
Minimum Range	0.5m	0.5m	0.25m
Maximum Range	20m (80% reflectivity) 7m (10% reflectivity)	10m (80% reflectivity) 7m (10% reflectivity)	8m (80% reflectivity) 5.5m (10% reflectivity)
Range Accuracy	$\pm 15\text{cm}$		
Frame Rate	5Hz, 10Hz, 15Hz, 20Hz, 25Hz		
Angular Resolution	0.1-1°		
Detection Layers	2		
Horizontal Field of View (HFOV)	50°	50°	100°
Vertical Field of View (VFOV)	4°		
Output Connection	100 Mbps Ethernet		
Data Outputs	Angle, Distance, Intensity		
Returns	1		
Ambient Light Immunity	Indoor	80,000 lux	80,000 lux
Nominal Power	9W		
Operating Voltage	9-30VDC		
Operating Temperature	-10°C to +50°C (+14°F to +122°F)		
Storage Temperature	-40°C to +70°C (-40°F to +158°F)		
Nominal Weight	671g (236g additional for optional heat sink)		
Dimensions	56mm (W) x 77mm (H) x 124mm (D)		
Environmental Protection	IP67		
Certifications and Compliance	FDA, FCC, CE, RoHS, WEEE		

Figure 3.9: S3-2 Specifications

3.4.6 Cube 1 (Blickfeld)

Cube 1 is a versatile 3D-LiDAR sensor that features an adaptable field of view, a configurable scan pattern, and a long-range while maintaining small dimensions and light weight. The proprietary solid-state technology is maintenance-free and durable. On-device pre-processing, an easy to use web user interface, and the associated recognition software makes Cube 1 a smart solution for numerous applications [13].

Cube 1's key specifications are presented in Figure 3.10.

Typical application range	1.5 – 75 m
Maximum detection range	250 m
Field-of-view (H x V)	70° x 30°
Vertical resolution	5 – 400 scan lines per frame (user-configurable)
Horizontal resolution	0.4° – 1.0° (user-configurable)
Operating voltage	12 V
Power consumption	less than 15 W
Laser class	Class 1, eye-safe (IEC 60825-1:2014, Ed. 3)

Figure 3.10: Cube 1 Specifications

Cube 1 is presented in Figure 3.11.



Figure 3.11: Cube 1

3.4.7 Cube Range 1 (Blickfeld)

The Cube Range 1 is made for extra-long-distance detection and offers high-precision 3D measurements. It features an adaptable field-of-view, a configurable scan pattern for versatile usage in various industries. No additional adapter boxes are required for operation and the point cloud interface ensures easy handling and configuration. On-device pre-processing and associated recognition software makes the Cube Range 1 a smart solution for numerous applications [13].

Cube Range 1's key specifications are presented in Figure 3.12.

Typical application range	5 – 150 m
Field of view (H x V)*	18° x 12°
Vertical resolution*	5 – 200 scan lines per frame
Horizontal resolution*	0.24° – 0.4°
Frame rate*	2.5 – 50 Hz; e.g. 15 Hz at 50 scan lines
Number of returns*	3
Dimensions (H x W x D)	60 mm x 82 mm x 86 mm
Weight	385 g
Power consumption	8.5 W
Laser class	Class 1, eye-safe (IEC 60825-1:2014, Ed. 3)

Figure 3.12: Cube Range 1 Specifications

Cube Range 1 is presented in Figure 3.13.



Figure 3.13: Cube Range 1

3.4.8 L515 (INTEL)

The Intel RealSense LiDAR Camera L515 uses an IR laser, a MEMS(micro-electro-mechanical systems), an IR(infrared) photodiode, an RGB imager, a MEMS controller, and a vision ASIC(application-specific integrated circuit). The MEMS is used to scan the IR laser beam over the entire field-of-view (FOV). The L515 vision ASIC will process the data from the reflected beam captured by the photodiode and will output a depth point representing the accurate distance of a specific point in the scene from the camera. Aggregation of the depth points will generate a point cloud depth data representing the full scene [14].

The specifications for the Intel RealSense LiDAR Camera L515 are presented in Figure 3.14.

Features	Use environment: Indoor Technology: Laser scanning	Ideal range: 25 m to 9 m ^[1] (Range affected by reflectivity)
Depth	Depth technology: LiDAR Minimum depth distance (Min-Z) at max resolution: ~25 cm Depth Accuracy: ~5 mm to ~14 mm thru 9 m ²	Depth Field of View (FOV): 70° × 55° (±3°) Depth output resolution: Up to 1024 × 768 Depth frame rate: 30 fps
RGB	RGB frame resolution: 1920 × 1080 RGB frame rate: 30 fps RGB sensor technology: Rolling Shutter	RGB sensor FOV (H × V): 70° × 43° (±3°) RGB sensor resolution: 2 MP
Major Components	Processing: Intel RealSense Vision ASIC	Optical board: – Laser – MEMS Mirror
Physical	Form factor: Camera Peripheral Diameter × Height: 61 mm × 26 mm	Connectors: USB-C® 3.1 Gen 1* Mounting mechanism: – One 1/4-20 UNC thread mounting point. – Two M3 thread mounting points. – Tripod

Figure 3.14: L515 Specifications

The L515 Camera is presented in Figure 3.15.



Figure 3.15: L515

3.4.9 4Sight M (AEYE)

4Sight M meets the diverse array of performance and functional requirements for the industrial and mobility markets with its industry-leading adaptive LiDAR performance, integrated intelligence, advanced vision capabilities, and unmatched reliability and safety. 4Sight M is a cost-effective, customizable perception solution that leverages the complete 4Sight software platform and includes a comprehensive SDK for an extensible roadmap to autonomous industrial and mobility applications [15].

The 4SIGHT and it's specifications are presented in Figure 3.16 and Figure 3.17 respectively.



Figure 3.16: 4Sight

LIDAR Specifications	4Sight™ M
Field of View	60° x 30° Baseline
Angular Resolution	0.1° horizontal (x) & vertical (y)
Triggerable Instantaneous Resolution	0.025°
User-Defined Frame Rate	Up to 200Hz
Software-Configurable Range	From 1cm to 1000m

Figure 3.17: 4Sight Specifications

3.4.10 OS0,OS1,OS2 (Ouster)

Ouster's [OS0](#), [OS1](#), and [OS2](#) spinning LiDAR units are available in 32-, 64-, and high resolution 128-channel designs. The differences between each model has to do with configuring the vertical field of view and angle to optimize performance for near-, mid- and long-field sensing needs. The OS0 features a wide 90° vertical field of view (VFOV). However, to achieve this, range is limited to 50m. The OS1 cuts VFOV in half to 45°, but in turn more than doubles effective range to 120m. The OS2 narrows VFOV to 22.5°, but range doubles to 240m.

The differences between each product with 128 channels and their specifications are presented in Figure 3.18.

Optical Performance			
Vertical resolution	128	128	128
Horizontal resolution	512, 1024, or 2048	512, 1024, or 2048	512, 1024, or 2048
Range (80% reflectivity)	50 m	120 m	240 m
Minimum range	.25 m	.25 m	.5 m
Vertical field of view	90°	45°	22.5°
Vertical angular resolution	0.7°	0.35°	0.18°
Precision	±1.5 - 5 cm	±0.7 - 5 cm	±2.5 - 8 cm
Rotation rate	10 or 20 Hz	10 or 20 Hz	10 or 20 Hz
Points per second	2,621,440	2,621,440	2,621,440
Number of returns	2 (strongest, second strongest)	2 (strongest, second strongest)	2 (strongest, second strongest)

Mechanical/Electrical			
Power consumption	14 - 20 W	14 - 20 W	18 - 24 W
Operating voltage	24 V nominal	24 V nominal	24 V nominal
Weight	447 g (with cap)	447 g (with cap)	1100 g (with cap)
Sensor height	73.5 mm (with cap)	73.5 mm (with cap)	98.9 mm (with cap)
Sensor diameter	85 mm	85 mm	119.6 mm
Connector styles	Straight, 90°	Straight, 90°	Straight, 90°
Interface options	Interface box, pig-tail cable	Interface box, pig-tail cable	Interface box, pig-tail cable
Laser Class	Class 1 Eye-Safe IEC/EN 60825-1:2014	Class 1 Eye-Safe IEC/EN 60825-1:2014	Class 1 Eye-Safe IEC/EN 60825-1:2014

Sensor output			
Beam configurations	Uniform	Uniform	Uniform
Embedded IMU	✓	✓	✓
Ambient (sunlight) imagery	✓	✓	✓
Time synchronization	PTP, \$GPRMC	PTP, \$GPRMC	PTP, \$GPRMC
Connection	UDP over gigabit Ethernet	UDP over gigabit Ethernet	UDP over gigabit Ethernet

Figure 3.18: OS0, OS1, OS2 Differences and Specifications

OS0, OS1 and OS2 are presented in Figure 3.19.



Figure 3.19: OS0, OS1 and OS2 (Left to Right respectively)

3.4.11 HPS-3D160 Pro, HPS-3D640 (Hypersen)

Based on Time-of-Flight(ToF) principle, integrating precise infrared lens and Laser illumination system, Hypersen 3D solid-state LiDAR can produce 3D point cloud data by just one shot and achieve real-time transmission through high-speed communication interface with embedded high-performance processor and professional algorithm. This LiDAR includes two models : [HPS-3D160 Pro](#) and [HPS-3D640](#) [16].

HPS-3D160 Pro and HPS-3D640 are presented in Figures 3.20-3.21 respectively.



Figure 3.20: HSP-3D160 Pro



Figure 3.21: HSP-3D640

Their differences are presented in Figure 3.22.

Model	HPS-3D160 Pro	HPS-3D640
Type	Solid-state	Solid-state
Measuring method	ToF	ToF
Resolution	160*60	640*480
Minimum resolution	1cm	1cm
FoV	76*32deg.	68*55deg.
Frame rate	35Hz/Adjustable	25Hz/Adjustable
Measuring range	0.25~3m @10% reflectivity 0.25~8m @90% reflectivity	0.25~2m @10% reflectivity 0.25~5m @90% reflectivity
Precision	±2cm	±1cm
Ambient Light Immunity	80,000Lux	80,000Lux
Communication interface	LAN, USB, USB-IO, RS-232(Slow)	LAN
Operating temperature	-10~+55°C	-10~+55°C
Power supply	12~24V	12~24V
Power consumption	3~5W	5~8W
Weight	110g	440g
Size	78*40*30mm	88*82*49mm

Figure 3.22: HSP-3D160 vs HSP-3D640

3.4.12 Leddar Pixell (LeddarTech)

Leddar Pixell enables dependable pedestrian detection and tracking as well as providing exceptional durability. Leveraging flash technology, Leddar Pixell illuminates and surveys the entire scene at once, enabling comprehensive detection capabilities over its 180° field of view. As such, this 3D solid-state LiDAR represents a powerful “detection cocoon” solution for ADAS and AD applications in commercial, public transit, military and off-road industrial vehicles [17].

Leddar Pixell and its specifications are presented in Figures 3.23-3.24 respectively.



Figure 3.23: Leddar Pixell

Description	Value	
Number of segments (H x V)	96 x 8	
Horizontal FoV	177.5°	
Vertical FoV	16°	
Angular resolution (horizontal)	1.9°	
Angular resolution (vertical)	2.0°	
Wavelength (nominal)	905 nm	
Frame rate	20 Hz	
Trueness⁵	± 5 cm	
Precision^{5, 6}	0.5 – 1 m: 1.5 cm 1 – 5 m: 1 cm 5 – 15 m: 5 cm 15 – 20 m: 11 cm > 20 m: 21 cm	
Demerging trueness⁷	± 10 cm	
Demerging precision^{6, 7}	8 cm	
Automotive connector	Mating cycle: 10 See section 7.2 on page 49 for more details.	
Automotive Ethernet	Physical layer (PHY) compliant with 100BASE-T1 (IEEE 802.3bw). Maximum length of 30 m. Leddar Pixell does not support the 802.3bp standard.	
Maximum bandwidth	Refer to Table 17 on page 45 for more details.	
Startup time	-30 °C	+20 °C
	≤ 15 s	≤ 6 s

Figure 3.24: Leddar Pixell's Specifications

3.4.13 AVIA (LIVOX)

The Livox Avia combines compact and lightweight design with improved detection range and efficiency, featuring an FOV greater than 70°. Its triple-echo and dual-scanning modes are ideal for use cases such as mapping, powerline surveying, smart cities and other applications [18].

Avia is presented in Figure 3.25.



Figure 3.25: Avia

3.4.14 CE30 (Benewake)

The Benewake CE30 LiDAR was developed especially for the industrial usage and is provided with a special hardware design. Both the groove width and the groove depth is, when compared with the competition, considerably larger and therefore enables a higher variety of possible applications. The main difference between the Benewake CE30 LiDAR types is the measurement range as well as the interfaces for data transmission. The CE30-A has a measurement range of 0,1-4m with a so called single point measurement through the CAN Bus. The CE-30D however has a measurement range of 0,1-30m, a UDP interface and a point cloud output format.

There are 3 different CE30 Models :

- CE30-A
- CE30-C
- CE30-D

The different models with theirs specs are presented in Figure 3.26.

Product	CE30-A	CE30-C	CE30-D
Appearance			
Performance	Range	0.1-4m	0.1-4m
	Pixel Resolution	320*24	320*24
	Distance Resolution	1cm	1cm
	Accuracy	≤6cm	≤6cm
	Repeatability	≤3cm	≤4cm
Weight	219g	219g	334g
Receiving Angle	132° x 9°	132° x 9°	60° x 4°
Electronics	Power	≤6W	≤8W
	Voltage	12V	12V
Communication	CAN	TCP/IP	UDP
Output	Nearest Obstacle Position (Single-Point Output)	Depth Image / Point Cloud	Point Cloud
Protection Level	IP65	IP65	IP65
Operating Temperature	0-50°C	0-50°C	0-50°C
Photobiological Safety	EN62471 Exempt	EN62471 Exempt	

Figure 3.26: CE30

3.4.15 Aeries (AEVA)

There are 2 different LiDARS that AEVA offers :

- Aeries I
- Aeries II

Aeries I is the first 4D LiDAR sensing system that meets perception requirements for the development and testing of autonomous vehicles and industrial programs. Leveraging a unique design of Frequency Modulated Continuous Wave (FMCW) technology, this all-in-one system combines LiDAR, camera, and processing electronics to output uniquely rich data that meets perception needs. Leveraging Aeva's unique Frequency Modulated Continuous Wave (FMCW) 4D technology and the world's first LiDAR-on-chip silicon photonics design, Aeries II's capabilities go beyond today's legacy Time-of-Flight LiDAR sensors.

Aeries I with its key features are presented in Figures 3.27-3.28.



Figure 3.27: Aeries I



Figure 3.28: Aeries I's Key Features

Aeries I with its key features are presented in Figures 3.29-3.30.

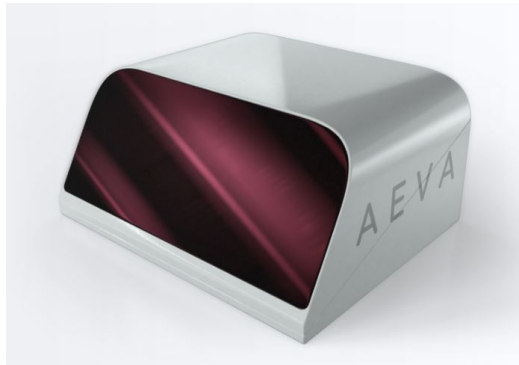


Figure 3.29: Aeries II



Figure 3.30: Aeries II's Key Features

3.4.16 Iris (Luminar)

Iris is a new kind of long-range lidar sensor, built from the chip level up. Iris is designed to meet the performance needs of autonomous vehicle manufacturers. Featuring a new form factor that can seamlessly integrate into vehicles, the company claims Iris is the first sensing platform to exceed the essential performance, safety, cost and auto-grade requirements needed to deliver Level 3 and 4 autonomy to consumers.

Iris is presented in Figure 3.31.



Figure 3.31: Iris

3.4.17 Sora-P Family (Cepton)

- Sora-P60

Sora-P60 is a best-in-class 380 Hz frame rate lidar that enables high fidelity object profiling at high speeds, for applications such as road tolling, vehicle and container scanning and similar applications.

Offering an exceptional combination of performance, reliability and affordability, it features an extremely compact and embedded design suitable for seamless integration into a wide range of smart systems [21].

- Sora-P90

Sora-P90 is Cepton's newest 90° field of view, 380 Hz frame rate lidar that enables high fidelity object profiling at high speeds, for applications such as road tolling, vehicle and container scanning and similar applications.

Offering an exceptional combination of performance, reliability and affordability, it features an extremely compact and embedded design with a wider field of view, suitable for seamless integration into a wide range of smart systems [21].

The Sora-P LiDARs are identical visually and are presented in Figure 3.32.



Figure 3.32: Sora Family

Sora-P60's and Sora-P90's specifications are presented in Figures 3.33-3.34.

Range
200 m at 30% reflectivity
Frame rate
380 Hz; 1140 lines/sec
FOV
60° (H) x 16° (V, 3 lines: +8°, 0°, -8°)
Resolution
0.22° (H)
Size
102 x 58 x 101 mm; 0.9 kg
Integration
PoE+ option available

Figure 3.33: Sora-P60 Specifications

Range
200 m at 80% reflectivity
Frame rate
380 Hz; 1140 lines/sec
FOV
90° (H) x 24° (V, 3 lines: +12°, 0°, -12°)
Resolution
0.35° (H)
Size
102 x 58 x 102 mm; 1.1 kg
Integration
PoE+ option available

Figure 3.34: Sora-P90 Specifications

3.4.18 Vista-X Family (Cepton)

- Vista-X90

Vista-X90 is a ground-breaking automotive grade lidar, attractively priced in automotive volumes. It sets a new benchmark for high performance at low power in a compact form factor and is ideally suited for advanced driver assistance systems (ADAS) and autonomous vehicles (AVs).

Optimized for ease of vehicle integration, the Vista-X90 has a licensable and modular design that enables configurability and manufacturability. The underlying MMT-based architecture is designed to meet the stringent requirements of automotive applications [22].

- Vista-X120

Vista-X120 is Cepton’s state-of-the-art lidar sensor delivering a wide horizontal field of view, high resolution and long range for autonomous driving, ADAS and other autonomous applications.

Offering an exceptional combination of performance, reliability and affordability, it enables seamless in-vehicle integration.

Vista-X90 and Vista-X120 are presented in Figures 3.35-3.36.



Figure 3.35: Vista-X90



Figure 3.36: Vista-X120

Vista-X90's and Vista-X120's specifications are presented in Figures 3.37-3.38.

Range
Up to 200 m at 10%
FOV
90° (H) x 25° (V)
Angular resolution
Up to 0.13° x 0.13°
Target Size
122 (W) x 46 – 63 (H, front-back) x 107 (D) mm; ~1 kg
Reliability / FuSa
Automotive grade, ISO-26262 ASIL-B

Figure 3.37: Vista-X90 Specifications

Range
Up to 200 m at 10%
FOV
120 (H) x 18-20 (V)
Angular resolution
Up to 0.13° x 0.13°
Target Size
130 (W) x 50 – 67 (H, front-back) x 110 (D) mm; ≤ 1.5 kg
Reliability
Automotive grade, ISO-26262 ASIL-B

Figure 3.38: Vista-X120 Specifications

3.4.19 Nova (Cepton)

Nova is our award-winning, miniature, wide field of view, near-range lidar sensor intended to address major gaps in proximity detection of objects with current sensor technologies.

Featuring best-in-class, high resolution 3D imaging with a high field of view (FOV), Nova sets a benchmark with its unprecedented combination of compactness, FOV coverage and affordability. It is ideally suited for advanced driver assistant systems (ADAS), autonomous vehicles (AVs), as well as autonomous ground vehicles (AGVs) and smart industrial applications [23].

Nova is presented in Figure 3.39.



Figure 3.39: Nova

Nova's Specifications are presented in Figure 3.40.

Range
Up to 30 m at 10% reflectivity
FOV
Up to 120° (H); up to 90° (V)
Angular resolution
Up to 0.3° x 0.3°
Target Size
50 (W) x 50 (H) x 100 (D) mm; <0.5 kg
Reliability / FuSa
Automotive grade, ISO-26262 ASIL-B

Figure 3.40: Nova Specifications

3.4.20 QT128 (Hesai)

QT128 is an ideal blind spot solution for L4 applications such as robotaxis and robotrucks. It has an industry-leading ultra-wide VFOV, allowing it to see more area. QT128 also has an automotive-grade design, giving it ultra-high reliability and long operating lifetime [24].

QT128 and its specifications are presented in Figures 3.41-3.42.



Figure 3.41: QT128

Vertical FOV 105.2° (-52.6° ~ +52.6°)	Instrument Range 0.1 ~ 50 m
Vertical Resolution Finest at 0.4°	Range Capability 20 m at 10% reflectivity
Horizontal FOV 360°	Range Accuracy ±3 cm
Horizontal Resolution Finest at 0.4° @10 Hz	Range Precision 2 cm
Working Temperature -40°C ~ 85°C	Data Points 864,000 pts/s
Power Consumption 12 W	Size (Top / Bottom x Height) Φ85.9 mm x Φ87.00 mm x H83.9 mm

Figure 3.42: QT128 Specifications

64-channel short-range LiDAR also available named as QT64.

3.4.21 AT128 (Hesai)

AT128 is a 128-channel ADAS LiDAR with a wide unstitched FOV of 120°, 200m effective detection and $0.1^\circ \times 0.2^\circ$ resolution, offering over 1.53 million data points per second. Both the LiDAR units and the components have gone through rigorous tests following international OEM standards [24].

AT128 and its specifications are presented in Figures 3.43-3.44.



Figure 3.43: AT128

1,536,000 points/s		
Data Points Generated		
200 m@10%	120° x 25.4°	0.1° (H) x 0.2° (V)
Range	Field of View	Resolution
17 W	137 mm x 112 mm x 47 mm	
Power Consumption	Dimensions	

Figure 3.44: AT128 Specifications

3.4.22 Pandar128 (Hesai)

128-channel, long-range (0.3 to 200 m), high-performance LiDAR with high reliability. Features Hesai's brand-new patented interference rejection technology. Horizontal resolution reaches 0.1° (10 Hz); data points up to 3,456,000 points/sec (single return). Image-like detection of surroundings [24].

Pandar128 and its specifications are presented in Figures 3.45-3.46.



Figure 3.45: Pandar128

Data Points Generated	Resolution
3,456,000 points/second (single return)	0.1° Finest horizontal resolution (10 Hz)
6,912,000 points/second (dual return)	0.125° Finest vertical resolution
Range Capability	Operating Temperature
200 m@10%	-40 – 85°C
*100 klux, PD>70%, FAR<1e ⁻⁵	
Accuracy	Ingress Protection
±2 cm (1 to 200 m)	IP6K9K & IP6K7
Functional Safety - compliant to ISO 26262	Cyber Security – compliant to ISO 21434
Comprehensive functional reporting for all lasers	Encryption to safeguard against data breaches

Figure 3.46: Pandar128 Specifications

64-channel LiDAR also available named as Pandar64.

3.4.23 XT32 (Hesai)

XT32 is Hesai's first LiDAR based on self-developed, proprietary LiDAR ASICs, resulting in enhanced product performance. Precision under typical conditions is up to 5 mm. Minimum range of zero. Suitable for applications including unmanned logistics and robotics [24].

XT32 and its specifications are presented in Figures 3.47-3.48.



Figure 3.47: XT32

Vertical FOV	Vertical Resolution	Horizontal Resolution
31° (-16° ~ +15°)	1°	0.18° @10 Hz
Range	Range Precision	Range Accuracy
0 m ~ 120 m 0 m calculated from LiDAR enclosure	0.5 cm <small>1σ precision</small>	±1 cm
Dimensions	Power Consumption	Data Points
100.0 mm <small>(Top Diameter)</small> 103.0 mm <small>(Bottom Diameter)</small> 76.0 mm <small>(Height)</small>	10 W	640,000 pts/s @Single return

Figure 3.48: XT32 Specifications

3.4.24 POWER-W (Genius-Pros)

- All-solid-state: No mechanical rotating parts in the interior to ensure higher reliability and stability
- Wide FOV: Simultaneously output 170° horizontal, 30° vertical field of view with gray and depth information
- Strong Scene Adaptability: Supports multi-devices collaboration with strong light resistance [25]

POWER-W is presented in Figure 3.49.



Figure 3.49: POWER-W

3.4.25 POWER-PBA2 (Genius-Pros)

- Full solid state: Without any moving parts
- High resolution: Can detect small obstacles
- Easy to fusion with camera: One shot (0.1ms/frame) Video rate (30FPS) [25]

POWER-PBA2 is presented in Figure 3.50.



Figure 3.50: POWER-PBA2

3.4.26 ULTRA-UGC1 (Genius-Pros)

- Full solid state: Without any moving parts
- High resolution and long detection range: Can detect small obstacles at long distances
- Easy to fusion with camera: One shot (0.1ms/frame) Video rate (30FPS) [25]

ULTRA-UGC1 is presented in Figure 3.51.



Figure 3.51: ULTRA-UGC1

3.4.27 ULTRA-UGC2 (Genius-Pros)

- Full solid state: Without any moving parts
- High resolution and long detection range: Can detect small obstacles at long distances
- Easy to fusion with camera: One shot (0.1ms/frame) Video rate (30FPS) [25]

ULTRA-UGC2 is presented in Figure 3.52.



Figure 3.52: ULTRA-UGC2

3.4.28 TetraVue 4D Flash LiDAR (tetravue)

For the first time, the multi-megapixel resolution and motion capture accuracy of digital video are combined with the range capability of LiDAR. TetraVue adds an entirely new fourth dimension of depth to digital video with the ability to capture accurate depth information at the pixel-level. This new camera technology is poised to transform markets including autonomous vehicles, machine vision, factory automation and the entertainment industry [26].

TetraVue 4D Flash LiDAR is presented in Figure 3.53.



Figure 3.53: TetraVue 4D Flash LiDAR

From what was researched the TetraVue 4D Flash LiDAR is still in development.

3.4.29 AX32 (ABAX SENSING)

AX32 series products are vehicle solid-state lidar , the receiving end of which is the focal plane distance sensor. The focal plane distance sensor receives the laser echo through the pixel unit inside the chip to generate the data that can be used to calculate the distance information, and to complete the point-cloud data collection inside the array by means of progressive scanning. The receiving end sensor adopts background eliminating technology, ultra-high dynamic range pixel-level implementation technology, laser cross-talk suppression and near-infrared enhancing technology [27]. The lidar products have four main characteristics as below:

- Low cost: adopting chip-level solution to reduce costs and the product size.
- High reliability: full solid-state FPA imaging technology, high environmental suitability and integration.
- High interference immunity: effectively dealing with interferences among different lidar equipment and disturbances by environmental lights.
- Eye safety: Speckle emission and focal plane receiving mode, protecting eyes from laser hazard.

AX32 is presented in Figure 3.54.



Figure 3.54: AX32

AX32 key features are presented in Figure 3.55 and the field of view probably makes it not applicable for our application.

- Angular resolution : $0.072^\circ \times 0.065^\circ$
- Field of view : $2.3^\circ \times 2.09^\circ$
- Range : 200m
- Range accuracy : 0.5%@200m
- Frame rate : >30fps

Figure 3.55: AX32 Specifications

3.4.30 OPAL-3 Conical/Panoramic (NeptecThechnologies)

The completely redesigned OPAL™ 3D LiDAR scanner from Lumibird is built from the ground up using the latest innovations in laser optics, detection technologies, and intelligent real-time 3D processing. The OPAL™ delivers an exceptional combination of detection range, data density, acquisition speed, and obscurant-penetrating capability in a smaller, lighter package.

The result is one of the most powerful and versatile 3D LiDAR scanners for robotics and autonomous systems specifically designed for operation in harsh and challenging environments.

OPAL™ scanners operate seamlessly with the 3DRi™ Software Development Kit (SDK), a library of proprietary algorithms to extract critical, actionable information from the scanners in real-time [28].

The OPAL-3 Conical and Panoramic models are presented in Figures 3.56-3.57.



Figure 3.56: OPAL-3 Conical



Figure 3.57: OPAL-3 Panoramic

The OPAL-3 Conical Model comes out with fields of view of $45^\circ, 60^\circ, 90^\circ, 120^\circ$.

3.4.31 InnovizOne (Innoviz Technologies)

InnovizOne is a solid-state LiDAR sensor specifically designed for automakers and robotaxi, shuttle and delivery companies requiring an automotive-

grade, mass-producible solution to achieve autonomy. The automotive-grade sensor is purpose-built to be rugged, affordable, reliable, low-power consuming, lightweight, high-performing and seamlessly integrable into Level 3-5 autonomous vehicles to ensure the safety of passengers and pedestrians alike [29].

InnovizOne is presented in Figure 3.58.



Figure 3.58: InnovizOne

3.4.32 InnovizTwo (Innoviz Technologies)

Innoviz has announced a new generation of its LiDAR sensor, InnovizTwo, which solves a significant bottleneck in the industry.

To allow a safer and smoother adoption of automation, the industry will need to introduce L2+ functionality with hardware that supports L3 and L4 upon launch. Due to its reduced cost and enhanced performance, InnovizTwo will allow more car manufacturers to offer safe L2+, while paving the path to full L3 automation in the most efficient and safe way.

With InnovizTwo, car manufacturers, Tier-1s and Innoviz will be able to collect data through their customer base. As new features will continue to be validated and, later, statistically proven. This dynamic will eventually lead to the car's software to be upgraded to full L3 without any hardware change [29].

InnovizTwo is presented in Figure 3.59.



Figure 3.59: InnovizTwo

3.4.33 Innoviz360 (Innoviz Technologies)

Innoviz360 is the next-generation high-performance 360° LiDAR for automotive and non-automotive applications from Innoviz. Its unsurpassed 3D perception performance is targeted at mass-production of Level 4 to Level 5 autonomous vehicles, as well as non-automotive industries including heavy machinery, smart cities, logistics and construction.

The rugged, reliable, functionally safe, and cost-effective LiDAR is lightweight, low-power, and resilient to sunlight and weather conditions. The sensor delivers a dense, highly accurate, 3D point cloud with unrivaled angular resolution at a high frame rate for distances up to 300m.

Innoviz360 supports pre-configured functionality including FOV scanning configuration with Region of Interest (ROI), pixel summation, frame rate, and multiple reflections [29].

Innoviz360 is presented in Figure 3.60.



Figure 3.60: Innoviz360

Innoviz360 samples will be available in Q4 2022.

3.4.34 InnovizPro (Innoviz Technologies)

InnovizPro offers outstanding performance and value for automotive, mapping, and other applications. It creates a dense 3D point cloud at a high frame rate that enables exceptional perception. InnovizPro offers high pixel density with uniform vertical field of view. The sensor's advanced design ensures reliability and resilience to sunlight and weather conditions.

InnovizPro is presented in Figure 3.61.



Figure 3.61: InnovizPro

3.4.35 Lumotive M30 (Lumotive)

The M30 mini-lidar targets applications in industrial and automotive markets. Its very small size ($<50\text{ cm}^3$), wide field of view of $120^\circ \times 90^\circ$ and low

power consumption (<6 W) are perfect for protecting the perimeter of a car or a mobile robot with up to 20 meter range [30].

Lumotive M30 is presented in Figure 3.62.



Figure 3.62: Lumotive M30

3.4.36 Lumotive U30 (Lumotive)

The U30 micro-lidar targets applications in consumer electronics markets. Its extremely small size ($<1\text{ cm}^3$), wide field of view (up to $120^\circ \times 90^\circ$) and low power consumption (<0.5 W) are perfect for integrating in mobile phones, AR goggles, or other demanding consumer electronics applications [30].

Lumotive U30 is presented in Figure 3.63.



Figure 3.63: Lumotive U30

3.4.37 Lumotive L30 (Lumotive)

The L30 long-range lidar targets demanding applications in automotive markets. It's long range, small size ($<400\text{ cm}^3$), wide field of view (up to $140^\circ \times 90^\circ$), high resolution ($0.1^\circ \times 0.1^\circ$), and high frame rate ($>20\text{ Hz}$) are perfect for detecting small targets with up to 200 m range at 10% target reflectivity.

Lumotive L30 is presented in Figure 3.64.



Figure 3.64: Lumotive L30

3.4.38 ML (SosLab)

ML(Mobility LiDAR) is the simplest LiDAR sensor in the world. It is a solid-state scanning type with no mechanical moving components which enables maximizing productivity in terms of mass production. With powerful performance and durability - yet compact and light, it can be used in various purposes for next-generation mobility [31].

ML is presented in Figure 3.65.



Figure 3.65: ML

ML has two different models and their specifications are presented in Figure 3.66.

FIELD OF VIEW	DETECTION RANGE	ANGULAR RESOLUTION	SCANNING FREQUENCY	ACCURACY
20°[H] x 10°[V] 180°[H] x 45°[V]	100m(@10%) 50m(@10%)	0.104°[H] x 0.2°[V] 0.5°[H] x 0.9°[V]	25fps	Up to ± 30mm

Figure 3.66: ML Specifications

3.4.39 XenoLidar Xact (Xenomatix)

The combination of high resolution and broad field of view makes it ideal for “exact” localization and classification of objects, outside or inside, in dynamic or static applications for automotive and non-automotive markets.

XenoLidar Xact is presented in Figure 3.67.



Figure 3.67: XenoLidar Xact

3.4.40 XenoLidar Xpert (Xenomatix)

With its long-range and high resolution it is ideally designed for (or “is an expert in”) focused safety and detection applications in automotive and non-automotive markets.

XenoLidar Xpert is visually identical with XenoLidar Xact but has different specifications which are presented in Table 4.

3.4.41 SP2.5/SP3.0 (Opsys)

Opsys flexible angular resolution and multiple base sensor architecture, allow customized FOV for each of our partners’ requirements. We constantly working to maximize our base sensor performances to achieve best in class results and promise safety, durability and scale. SP2.5 SP3.0 represent our development plan for the coming year [33].

SP2.5 and SP3.0 are presented in Figures 3.68 and 3.69 respectively.



Figure 3.68: SP2.5



Figure 3.69: SP3.0

3.4.42 Spectrum HD (Baraja)

From the windshield to over 250m away, the Spectrum-Scan system has unrivaled object detection at long range – giving self-driving vehicles precious seconds to make safety-critical decisions at high speeds. While other LiDAR makers are still solving scanning issues, we’re continually improving the precision of our pointcloud to create trusted data that’s reliable enough for the next milestone in vehicle automation. Dependable sensor data that depicts the real world and is immune to interference from both the environment and other LiDAR sensors [34].

Spectrum HD is presented in Figure 3.70.



Figure 3.70: Spectrum HD

3.4.43 Spectrum Off-Road (Baraja)

Developed alongside one of our trusted mining partners, Spectrum Off-Road is where Spectrum-Scan technology meets the toughest standards in durability, ruggedization and reliability. With a field-tested, inherently reliable scanning mechanism, Spectrum-Scan technology meets comprehensive independent testing and verification for shock resistance, longevity, and operation in the harshest environments [34].

Spectrum Off-Road is presented in Figure 3.71.

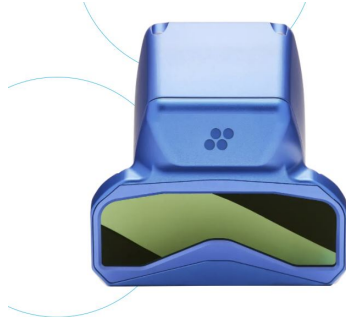


Figure 3.71: Spectrum Off-Road

3.4.44 ibeoNEXT (Ibeoautomotive)

The ibeoNEXT Fusion System for environmental perception consists of two main components: The lidar sensors and the electronic control unit (ECU). The sensors are available with a 11.2 degree or 60 degree optic (32 degree and 120 degree optics are currently under development). They can be installed or mounted in any preferred way – depending on your use case. The sensor functionality is not limited to the application shown in this example. The ECU includes our proprietary perception software to process the data. Via the visualization software, the integrated point cloud, the intensity image and the 3D object tracking are displayed [35].

IbeoNEXT is presented in Figure 3.72.



Figure 3.72: ibeoNEXT

3.4.45 ibeo LUX (Ibeoautomotive)

The ibeo LUX lidar sensor scans the area around the sensor and uses lasers to detect any objects that are present in its field of view. The mirror inside the

sensor constantly rotates, deflecting a laser beam to scan the environment and create a comprehensive image of the entire space in the laser's field of view. The scan data of the ibeo LUX comprise distance, angle, and echo pulse width. The ibeo LUX allows for detection of the environment in a field of view of 110 degrees and at a distance of up to 200 meters [35].

IbeoLUX is presented in Figure 3.73.



Figure 3.73: ibeoLUX

IbeoLUX has 3 different models :

- ibeo LUX 4L
- ibeo LUX 8L
- ibeo LUX HD

Their specifications are presented in Figure 3.74.

LASER / OPTICAL	ibeo LUX 4L	ibeo LUX 8L	ibeo LUX HD
Laser class:		Class 1	
Wave length:		905 nm	
Technology:		Time of flight, Output of distance and echo pulse width	
Range:	50 m / 164 ft @ 10% remission	50 m / 164 ft @ 10% remission	30 m / 98 ft @ 10% remission
MEASUREMENT	ibeo LUX 4L	ibeo LUX 8L	ibeo LUX HD
Horizontal field of view:		110° (50° to -60°)	
Vertical field of view:	3.2°	6.4°	3.2°
Multi-layer:	4 parallel scanning layers	8 layers (2 pairs of 4 layers)	4 parallel scanning layers
Multi echo:		Up to 3 distance measurements per shot (allow measurements through atmospheric clutter like rain and dust)	
Data update rate:		25.0 Hz	
Operating temperature range:		-40° to 85° C / -40° to 185° F	
Accuracy (distance independent):		10 cm / 3.9 in	
Angular resolution:		Horizontal: up to 0.25° Vertical: 0.8°	
Distance Resolution:		4 cm / 1.57 in	
SOFTWARE	ibeo LUX 4L	ibeo LUX 8L	ibeo LUX HD
Raw data pre-processing (embedded):		All measurements will be classified and tagged as valid / ground / clutter	
Real time object tracking (embedded):		Object properties: position, size, speed	
Ego motion compensation (embedded):		Requires vehicle ego motion data	
Fusion:		Fusion of multiple sensors (LUX 4L, 8L, HD) for 360° FOV is possible	
MECHANICAL / ELECTRICAL	ibeo LUX 4L	ibeo LUX 8L	ibeo LUX HD
Power supply:		9 to 27 V	
Power consumption:	7 W (average), <10 W (max)	8 W (average), <10 W (max)	7 W (average), <10 W (max)
Dimensions (WxDxH):		164.5 x 93.2 x 88 mm 6.47 x 3.67 x 3.46 in	
Protection class:		IP 69K (IEC 60529, DIN 40050-9 (using protected plug connectors)) IP 68 (IEC 60529 (2 m, 24 h))	
DATA I / O	ibeo LUX 4L	ibeo LUX 8L	ibeo LUX HD
Ethernet:		Output: Raw- and object data Input: Configuration / time sync via NTP server	
CAN :		Output: Object data Input: Ego motion data	
RS232:		Sync	

Figure 3.74: ibeoLUX Specifications

3.4.46 Dynamic View LiDAR or A-Sample (Microvision)

MicroVision's lidar sensor delivers high resolution at range, detecting smaller objects from longer distances and identifying them clearly. The ability of our technology to provide resolutions as low as 0.03 degrees ranging up to 250 meters will improve path planning for customers focusing on autonomous driving or allow ADAS safety measures to be applied quickly, even at highway speeds.

With our lidar sensor's ability to measure and report the velocity of objects in any scenario—laterally and axially—we can understand their paths and help predict their trajectories. Our sensors update the position and velocity of moving objects 30 times per second. This enables fast and accurate path planning to anticipate where objects will end up and improve driver safety.

MicroVision's lidar sensor will work across a range of ambient environments, from bright sunlight to nighttime driving conditions. Our sensor is free of interference from all other lidars. This is achieved through our proprietary technology that provides immunity from all types and wavelength lidar products [36].

Key feature of Microvision's LiDAR is it's immunity to sunlight.

The A-Sample LiDAR is presented in Figure 3.75.



Figure 3.75: A-Sample LiDAR

3.5 Differences

Model	Min/Max Range at % Reflectivity	Output	Range Accuracy	Precision/Repeatability	Field of View (H x V)	Price
Velarray H800 (Velodyne)	0.1m/200m at 10%	PointCloud	0.1m	Unknown	(120°x16°)	\$500.00
Velarray M1600 (Velodyne)	0.1m/30m at 10%	PointCloud	0.1m	Unknown	(120°x35°)	(Awaiting Response)
Velabit (Velodyne)	Unknown/100m at 10%	PointCloud	Unknown	Unknown	(90°x70°)	\$100.00 (Target)
RS-LiDAR-M1 (Robosense)	0.5m/120m at 10%	PointCloud	±0.05m	Unknown	(120°x25°)	\$1,898.00
S3-2NSI-S00 (Quanergy)	0.5m/20m at 80%	PointCloud	±0.15m	Unknown	(50°x4°)	\$500.00 (Target)
S3-2NSO-S00 (Quanergy)	0.5m/10m at 80%	PointCloud	±0.15m	Unknown	(50°x4°)	\$500.00 (Target)
S3-2WSO-S00 (Quanergy)	0.25m/8m at 80%	PointCloud	±0.15m	Unknown	(100°x4°)	\$500.00 (Target)
Cube 1 (Blickfeld)	1.5m/250m (>30m for 10%)	PointCloud	< 0.01m (Range Resolution)	< 0.02m	(70°x30°)	€3,500.00
Cube Range 1 (Blickfeld)	5m/250m (>50m for 10%)	PointCloud	< 0.01m (Range Resolution)	Unknown (Probably < 0.02m)	(18°x12°)	€3,500.00
L515 (INTEL)	0.25m/9m at 95%	PointCloud	< 0.02m	High Precision (No Measurement Found)	(70°x43°)	€581.42
4Sight M (AEYE)	0.01m/1000m(>120m for 10%)	PointCloud	±0.025m	Unknown	(60°x30°)	\$1,000.00
OS0-32 (Ouster)	0.25m/20m at 10%	PointCloud	±0.03m	±0.01m to ±0.05m	(360°x90°)	\$6,000.00
OS1-32 (Ouster)	0.25m/40m at 10%	PointCloud	±0.03m	±0.007m to ±0.05m	(360°x45°)	\$6,000.00 (For University Research)
OS2-32 (Ouster)	0.5m/240m at 80%	PointCloud	±0.03m±0.025m to ±0.08m		(360°x22.5°)	\$16,000.00
HSP-3D160 (Hypersen) Pro	0.25m/8m at 90%	PointCloud	Unknown	±0.02m	(76°x32°)	\$329.00
HSP-3D640 (Hypersen)	0.25m/5m at 90%	PointCloud	Unknown	±0.01m	(68°x55°)	€1,649.95
Leddar Pixell (LeddarTech)	0.5m/56m at 80%	PointCloud	±0.05m	±0.03m (Average) (Close Range)	(177.5°x16°)	\$2,400.00
AVIA (Livox)	1m/450m at 80%	PointCloud	0.05m	0.02m	(70.4°x77.2°)	€1,399.00
CE30-A (Benewake)	0.1m/4m at 90%	PointCloud	≤ 0.06m	≤ 0.03m	(132°x9°)	€794.95
CE30-C (Benewake)	0.1m/4m at 90%	PointCloud	Unknown	Unknown	(132°x9°)	€1,040.06
CE30-D (Benewake)	0.4m/30m at 90%	Nearest Obstacle Position	0.15m	0.05m	(60°x4°)	€1,718.95
Aeries I (AEVA)	0.4m/28m at Unknown	PointCloud	Unknown	Unknown	(60°x4°)	Unknown
Aeries II (AEVA)	0.4m/28m at Unknown	PointCloud	Unknown	Unknown	(60°x4°)	Unknown
Iris (Luminar)	Unknown/600m (≥250m at 10%)	PointCloud	Unknown	0.01m	(120°x26°)	\$1,000.00 (Target)

Table 2: Prices

Model	Min/Max Range at % Reflectivity	Output	Range Accuracy	Precision/Repeatability	Field of View (H x V)	Price
Sora-P60 (Cepton)	Unknown/200m at 30%	PointCloud	Unknown	Unknown	(60°x16°)	(Awaiting Response)
Sora-P90 (Cepton)	Unknown/200m at 80%	PointCloud	Unknown	Unknown	(90°x24°)	(Awaiting Response)
Vista-X90 (Cepton)	Unknown/200m at 10%	PointCloud	Unknown	Unknown	(90°x25°)	(Awaiting Response)
Nova (Cepton)	Unknown/30m at 10%	PointCloud	Unknown	Unknown	(120°x90°)	(Awaiting Response)
QT128 (Hesai)	0.1m/20m at 10%	PointCloud	±0.03m	Unknown	(360°x105.2°)	(Awaiting Response)
AT128 (Hesai)	0.5m/200m at 10%	PointCloud	±0.06m/(0.5m ~ 3m), ±0.02m/(3m ~ 200m)	Unknown	(120°x25.4°)	(Awaiting Response)
Pandar128 (Hesai)	0.3m/200m at 10%	PointCloud	±0.02m	Unknown	(360°x40°)	(Awaiting Response)
X132 (Hesai)	0.80m at 10%	PointCloud	±0.01m	Unknown	(360°x31°)	(Awaiting Response)
POWER-W (Genius-Pros)	Unknown/8m at 10%	PointCloud	±0.1m	2%	(170°x30°)	(Awaiting Response)
POWER-PBA2 (Genius-Pros)	0.5/20m at Unknown%	PointCloud	0.5%~1%	1%	(70°x40°)	(Awaiting Response)
ULTRA-UGC1 (Genius-Pros)	Unknown/40m at 10%	PointCloud	0.5%~1%	1%	(40°x20°)	(Awaiting Response)
ULTRA-UGC2 (Genius-Pros)	Unknown/100m at 10%	PointCloud	0.5%~1%	1%	(25°x8°)	(Awaiting Response)
OPAL Conical (Neptec Technologies)	Unknown/500m at 20%	PointCloud	≤ 0.02m	≤ 0.02m	(120°x120°)	(Awaiting Response)
OPAL Panoramic (Neptec Technologies)	Unknown/500m at 20%	PointCloud	≤ 0.035	≤ 0.02m	(360°x45°)	(Awaiting Response)
InnovizOne (Innoviz Technologies)	0.1/250m at Unknown%	PointCloud	Unknown	Unknown	(115°x25°)	(Awaiting Response)
InnovizTwo (Innoviz Technologies)	0.3/300m at Unknown%	PointCloud	Unknown	Unknown	(120°x40°)	(Awaiting Response)
Innoviz360 (Innoviz Technologies)	0.3/300m at Unknown%	PointCloud	Unknown	Unknown	(360°x64°)	(Awaiting Response)
InnovizPro (Innoviz Technologies)	2.1/60m at 10%	PointCloud	0.05m	Unknown	(72°x18.5°)	(Awaiting Response)
Lumotive M30 (Lumotive)	Unknown/20m at Unknown%	PointCloud	Unknown	Unknown	(120°x90°)	(Awaiting Response)
Lumotive U30 (Lumotive)	Unknown/10m at Unknown%	PointCloud	Unknown	Unknown	(120°x90°)	(Awaiting Response)
Lumotive L30 (Lumotive)	Unknown/200m at 10%	PointCloud	Unknown	Unknown	(140°x90°)	(Awaiting Response)

Table 3: Prices

Model	Min/Max Range at % Reflectivity	Output	Range Accuracy	Precision/Repeatability	Field of View (H x V)	Price
ML-0 (SosLab)	Unknown/100 at 10%	PointCloud	± 0.03	Unknown	$(20^\circ \times 10^\circ)$	(Awaiting Response)
ML-2 (SosLab)	Unknown/50m at 10%	PointCloud	± 0.03	Unknown	$(180^\circ \times 45^\circ)$	(Awaiting Response)
XenoLidar Xact (Xenomatix)	Unknown/50m at Unknown%	PointCloud	Unknown	Unknown	$(60^\circ \times 20^\circ)$	(Awaiting Response)
XenoLidar Xpert (Xenomatix)	Unknown/150m at Unknown%	PointCloud	Unknown	Unknown	$(30^\circ \times 10^\circ)$	(Awaiting Response)
SP2.5 (Opsys)	Unknown/150m at 10%	PointCloud	Unknown	Unknown	$(22.5^\circ \times 13^\circ)$	(Awaiting Response)
SP3.0 (Opsys)	Unknown/200m at 10%	PointCloud	Unknown	Unknown	$(22.5^\circ \times 13^\circ)$	(Awaiting Response)
Spectrum HD (Baraja)	0.01m/220m at 10%	PointCloud	$\pm 2\%$ pts	$\pm 4\%$ pts	$(120^\circ \times 25^\circ)$	$\leq \$1,000.00 (Target)$
Spectrum Off-Road (Baraja)	Unknown/Unknown at Unknown%	PointCloud	Unknown	Unknown	$(120^\circ \times 30^\circ)$	Unknown
ibeoNEXT (ibeoautomotive)	Unknown/140m at 10%	PointCloud	Unknown	Unknown	$(120^\circ \times 60^\circ)$	(Awaiting Response)
ibeolUX 4L (ibeoautomotive)	0.3m/50m at 10%	PointCloud	0.04m	Unknown	$(110^\circ \times 3.2^\circ)$	(Awaiting Response)
ibeolUX 8L (ibeoautomotive)	0.3m/50m at 10%	PointCloud	0.04m	Unknown	$(110^\circ \times 6.4^\circ)$	(Awaiting Response)
ibeolUX HD (ibeoautomotive)	0.3m/30m at 10%	PointCloud	0.04m	Unknown	$(110^\circ \times 3.2^\circ)$	(Awaiting Response)
ibeolUX HD (ibeoautomotive)	0.3m/30m at 10%	PointCloud	0.04m	Unknown	$(110^\circ \times 3.2^\circ)$	(Awaiting Response)
A-Sample (Microvision)	Unknown/250m at 10%	PointCloud	Unknown	Unknown	$(100^\circ \times 25^\circ)$	$\leq \$1,000.00$

Table 4: Prices

4 LiDAR Introduction

LiDARs use electromagnetic (EM) waves in the optical and infrared wavelengths. It is an active sensor, meaning that it sends out an EM wave and receives the reflected signal back. Because it has a much shorter wavelength than a microwave radar, it will have much better angular resolution but it will not see through fog or clouds. LiDARs use their own flashlight and can therefore see at night. This means that LiDAR can have increased angular resolution associated with the shorter wavelengths and still operate 24 hours per day.

The relationship between wavelength and frequency is :

$$c = \lambda * v \quad (1)$$

where c is the speed of light, λ is the wavelength and v is the frequency. If the wavelength of an EM wave is significantly longer than the particle size, the wave just flows around particles with little or no attenuation. A 30-cm (or even a 3-cm) microwave signal is significantly larger than rain droplets so will not be significantly attenuated by fog or rain. Millimeter waves at 95 GHz have a wavelength larger than fog but smaller than many rain droplets, so they see through fog well, but not as well through some rain. Fog is worse for LiDAR than rain because fog is made of more particles. The color of an object can be measured if more than one wavelength of light is used in the LiDAR. Velocity can be measured either directly using the Doppler shift—the Doppler effect or Doppler shift (or simply Doppler, when in context) is the change in frequency of a wave in relation to an observer who is moving relative to the wave source—in frequency due to motion, or by multiple measurements of position.

The Doppler shift changes the frequency of the return laser signal based on :

$$\Delta f = \frac{2V}{\lambda} \quad (2)$$

where V is the velocity and λ is the wavelength.

Micro-motion can be measured using the Doppler shift, which is usually measured with a coherent LiDAR. A coherent LiDAR beats the return signal

against a local oscillator (LO), which is a sample of the outgoing laser signal. This allows us to measure the phase of the return signal. LiDAR is a great sensor for identifying objects. One of the reasons for this is that LiDAR can operate at wavelengths similar to what the eye is used to seeing. A LiDAR can provide a 2D angle/angle image but can also provide a 3D image with angle/angle/range information. A LiDAR can directly measure range in each pixel because it controls when light is emitted so can measure range based on time of flight to and from the object in a given pixel. A waveform generator creates the laser waveform needed to obtain range or velocity information. A laser would usually provide the illumination, although it is possible to have a LiDAR without a laser. There needs to be a transmit optical aperture that emits the light. This can be the same aperture as the receive aperture, or a different aperture. If it is the same aperture, we call it a monostatic LiDAR, where mono means one aperture. If the transmit and receive apertures are different, we call it a bistatic LiDAR, meaning two apertures. Light has to traverse a medium, usually atmosphere, to arrive at a target. LiDAR can be transmitted through the vacuum of space. LiDAR can also be used through water instead of air or space. The conceptual diagram of a LiDAR is presented in Figure 4.1.

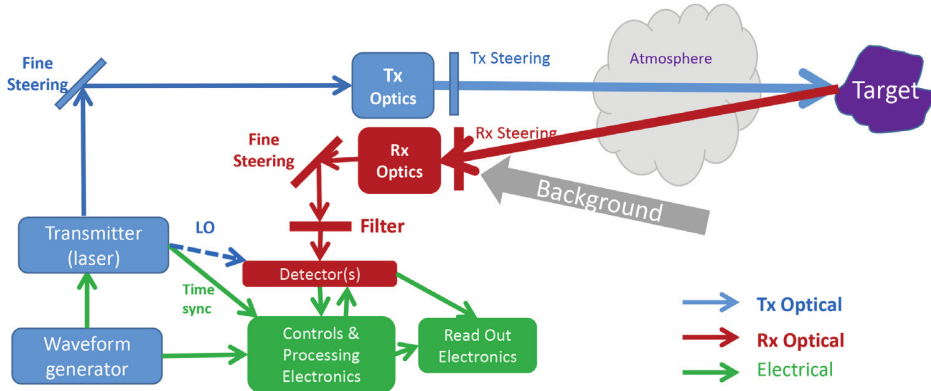


Figure 4.1: LiDAR Conceptual Diagram

LiDAR light bounces off the target and traverses the medium again until it is captured by the receiver optical aperture in the pupil plane, which also needs to point at the target. If we use a lens to focus the light captured by the receive aperture, then we convert to the image plane. Alternatively, if we can capture or estimate the field at the aperture (the pupil plane), we

can Fourier transform the field at the pupil plane to form an image. One of the nice things about capturing the full field (phase and intensity) in the pupil plane is that a larger pupil-plane aperture can be synthesized and then Fourier transformed to make a higher-resolution image. To measure the full field in the pupil plane rather than just the intensity requires that we beat the return signal against another signal that (as mentioned) we call the local oscillator (LO)—a local oscillator (LO) is an electronic oscillator used with a mixer to change the frequency of a signal. This frequency conversion process, also called heterodyning, produces the sum and difference frequencies from the frequency of the local oscillator and frequency of the input signal. To detect temporal phase, we can use an LO that interferes with the return signal on the detector. We refer to the LO beating against the return signal. We can then measure the beat frequency, which allows us to measure the phase of the return light as well as the intensity (we call this coherent LiDAR). If the LO is perfectly stable, the phase change in the beat frequency is the same as the phase of the carrier frequency, which is the returned signal, so in coherent LiDAR, we can capture phase. We need a timing signal from the transmitter to determine range by measuring time of flight of the laser pulse to and from the target. We know the speed of light in vacuum and in air, so we can calculate the distance to an object. The signal generated by the detector is digitized and then processed to make an image or to generate information such as velocity or vibration frequency based on the return Doppler shift.

4.1 Types of LiDARs

Range in a LiDAR is measured by timing how long it takes light to hit an object and return. Range resolution is given by :

$$\boxed{\Delta R = \frac{c}{2B}} \quad (3)$$

where ΔR is the range resolution, c is the speed of light in the intervening medium and B is the system bandwidth.

Angular resolutions can either be limited by the detector angular subtense (DAS, The measured planar or solid angle of related aspects of an optical system with respect to an optical axis.) or by diffraction—Laser diffraction analysis, also known as laser diffraction spectroscopy, is a technology that

utilizes diffraction patterns of a laser beam passed through any object ranging from nanometers to millimeters in size to quickly measure geometrical dimensions of a particle. Figure 4.2 shows various sampling possibilities; the middle curve represents the case where the DAS is about the same as the point spread function (PSF) of the optical aperture. We could also over-sample the PSF as shown on the right, or under sample it as shown on the left.

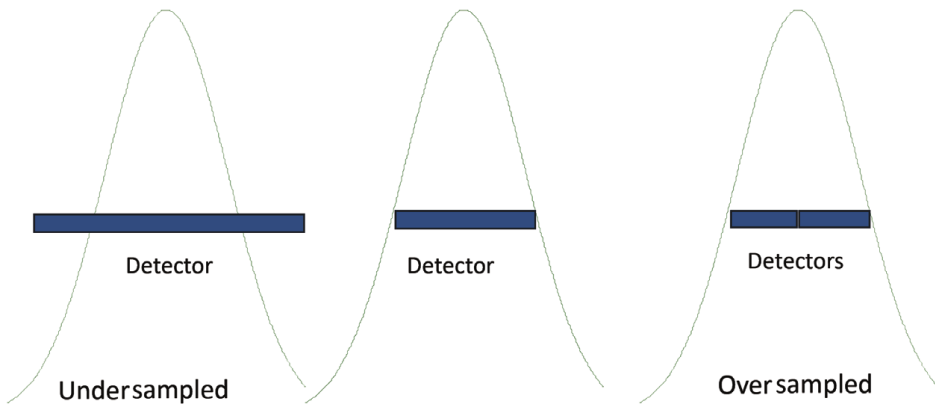


Figure 4.2: LiDAR Sampling Possibilities

4.2 LiDAR Detection Modes

When light hits a detector, it generates a voltage equal to the square of the intensity of the impinging light. In ideal direct detection, only the LiDAR return hits the detector, causing a response equal to the square of the intensity of the impinging light. In coherent LiDAR, the return signal beats against a sample of the emitted signal, which we call the local oscillator (LO). In this case, the detector can respond to the real portion of the beat frequency, or difference frequency, between the return signal and the LO:

$$I = 2E_{sig}E_{LO}\cos[-j(\omega_{sig} - \omega_{LO})] \quad (4)$$

If the LiDAR uses a detector array, which we refer to as flash LiDAR, then the laser illuminates an area as large in angle as the detector array, so the laser beam is wider in angle. The diffraction limit provides the smallest possible

laser beam divergence. The full beam width, half maximum diffraction limit is :

$$\theta \approx \frac{1.03\lambda}{D} \quad (5)$$

where D is the diameter of the transmit aperture.

4.3 Monostatic versus Bistatic LiDAR

If the transmit and receive apertures are two separate apertures, we call that a bistatic LiDAR, as shown in Fig. 1.13. The transmit, or illumination, aperture does not have to be the same size as the receive aperture, nor in the same place.

One reason for using monostatic LiDARs is to save weight and space by not having a second aperture for illumination; however, with bistatic illumination often you can have an illumination aperture that is much smaller than the receive aperture, reducing the size, weight, and power impact of having two apertures. This is the case for flash LiDAR, where the area illuminated is larger than the area viewed by a single DAS.

Also, as will be discussed in Chapter 4, multiple-input, multiple-output (MIMO) LiDARs provide the benefits of having more than one transmitter and more than one receiver. Any MIMO LiDAR is inherently bistatic. Often in a MIMO LiDAR, the transmit apertures will be smaller than the receive apertures.

4.4 Transmit/Receive Isolation

One way to isolate the receiver from the transmitter is to have a bistatic LiDAR with separate apertures. If the LiDAR has a pulsed-cycle, or low-duty cycle, transmitter, then another way to isolate the receiver from the transmitter is to keep the receiver off while the laser is transmitted. Figure 4.3 presents the transmit/receive isolation approach using polarization.

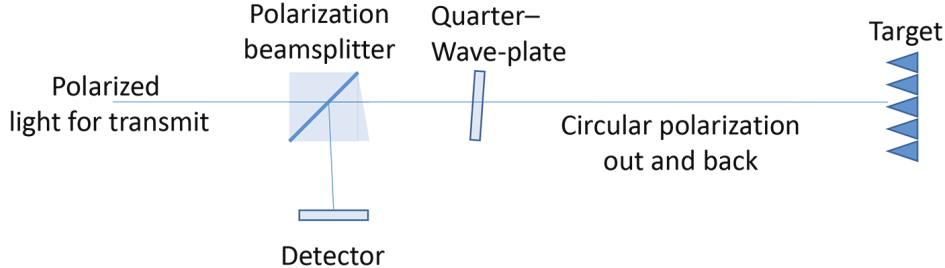


Figure 4.3: Transmit/Receive Isolation Using Polarization

5 LiDAR Range Equation

To calculate the required energy, or power, to obtain a measurable return with a LiDAR, the calculation can be divided into two parts. The first part is the calculated intensity of the reflected laser light from the target. This result can be stated in terms of the number of photons returned to each detector in a certain period of time. The second part calculates how much energy, in photons, is needed in each detector to measure the returned signal. For the second part, the returned energy to the noise have to be compared.

5.1 Illuminator Beam

To calculate the number of photons returned to each detector, an engineer can start with the transmitted laser power. The transmitter can have a beam shaped as a Gaussian beam or a super-Gaussian, or it can be a flat-top beam.

The full-angular-width, half-maximum diffraction limit θ is given by :

$$\boxed{\theta \approx \frac{\lambda}{D}} \quad (6)$$

where λ is the wavelength, and D is the beam diameter. For transmitters, the beam diameter has to be smaller than the transmit aperture diameter to avoid significant clipping. Figure 5.1 shows a Gaussian beam compared to a super-Gaussian beam with $N = 5$. The equation for the Gaussian beam is :

$$\boxed{f(x) = ae^{-\frac{(x-b)^2}{2c^2}}} \quad (7)$$

whereas a super-Gaussian beam shape is given by :

$$f(x) = ae^{-\frac{(x-b)^N}{2c^2}} \quad (8)$$

In both Equations 7 and 8, a is the amplitude of the Gaussian beam, c is a measure of the width, and b is an offset.

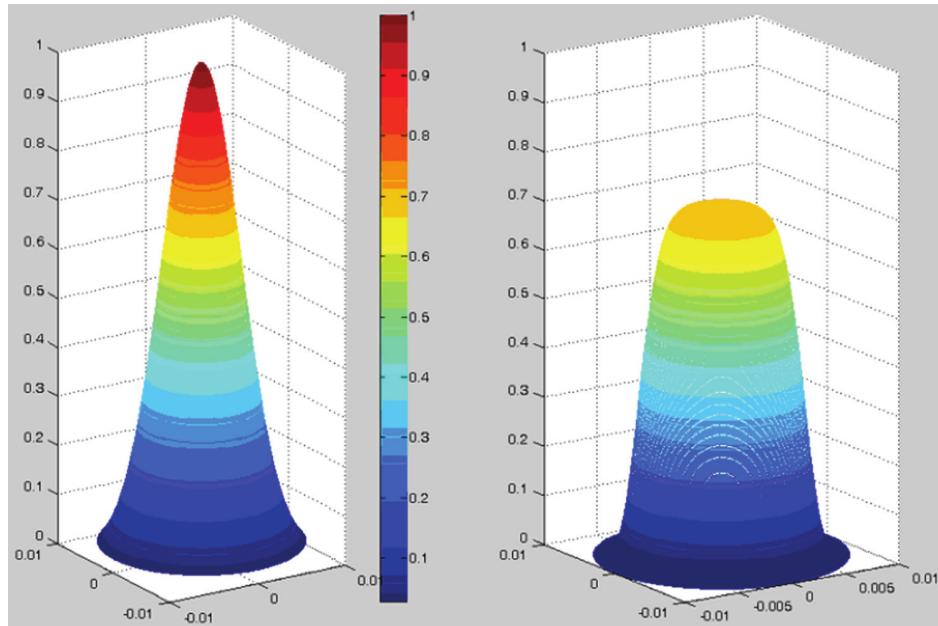


Figure 5.1: The shape of (left) a Gaussian beam compared to a super-Gaussian beam (right) with $N = 5$

Beams that are more flat topped have less clipping at the apertures. Clipping of the Gaussian beam is shown in Figure 5.2.

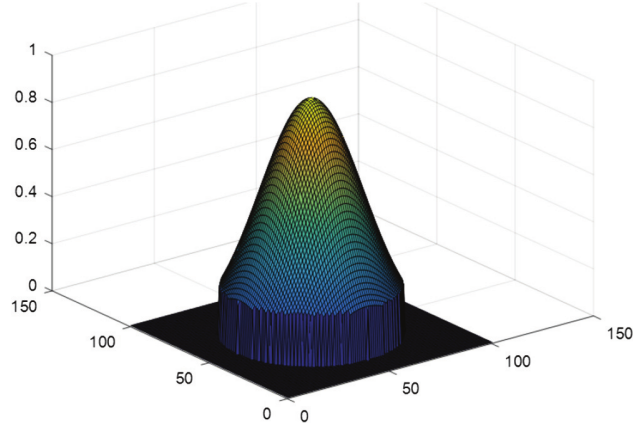


Figure 5.2: Clipped Gaussian beam with $c = 1$ and aperture diameter = 2.5

5.2 LiDAR Cross-Section

Next a fictitious area is created which is called the cross-section. This is not a physical area but is related to the physical area. For area targets, with a flash- imaging LiDAR, by using many detectors, cross- sections can be counted only if they are seen by each detector when calculating cross-section because how much power, or energy, is calculated that is being reflected into a given detector. For a target whose illumination area is larger than the detector angular subtense (DAS), we can assume that the cross-section viewed by a receiver pixel is proportional to the projected area of a pixel times the reflectance. For square receiver pixels, we have :

$$\boxed{\sigma = \rho_t A_p = \rho_t d^2} \quad (9)$$

where d is length of one side of the projected area of a pixel on the target, ρ_t is the reflectance of the area, and A_p is the area of the pixel, which for a square pixel is d^2 .

The area seen by the detector grows with range according to :

$$\boxed{\sigma = \rho_g x (DAS)^2 x R^2} \quad (10)$$

where ρ_g is the ground reflectivity and $DASxR = d$ in Equation 9.

5.3 Power Calculation

The power received in a given detector can be calculated using :

$$P_R = P_T \frac{c}{A_{illum}} \frac{A_{rec}}{\pi R^2} n_{atm}^2 n_{sys} \quad (11)$$

where P_R is the power received, P_T is the power transmitted, σ is the cross-section in square meters, A_{illum} is the area illuminated, A_{rec} is the area of the receiver, R is the range, n_{atm} is the transmission efficiency through the atmosphere, and n_{sys} is the receiver system's optical efficiency.

5.4 Atmospheric Losses

One of the main loss factors in the LiDAR equation is atmospheric loss, and much of that loss comes from scattering. We have three main regimes of scattering: where the particle is much smaller than the EM wavelength, where the particle is on the order of the same size as the EM wavelength, and where the particle is much larger than the EM wavelength. Rayleigh scattering (Fig. 3.10) is the elastic scattering of light by molecules and particulate matter that are much smaller than the wavelength of the incident light. Rayleigh scattering intensity is proportional the sixth power of the diameter of the scattering particle and inversely proportional to the fourthpower of the wavelength of light. This means that the shorter wavelengths in visible light (violet and blue) are scattered more strongly than the longer wavelengths toward the red end of the visible spectrum. This scattering is responsible for the blue color of the sky during the day and the orange colors during sunrise and sunset.

5.5 Atmospheric Turbulence

Because of small variations in the index of refraction of the air, there is a maximum effective aperture size on receive when a LiDAR is looking through the atmosphere, and on transmit through the atmosphere. This will limit the diffraction-limited resolution of a LiDAR unless turbulence is compensated. While these index-of-refraction variations are small (on the order of 0.0001 or less) they cause phase changes across an aperture. The largest diameter

that an aperture can have without corruption due to phase variations is called the Fried parameter r_0 . Figure 5.3 shows a beam transmitting through atmosphere that has turbulence variations.

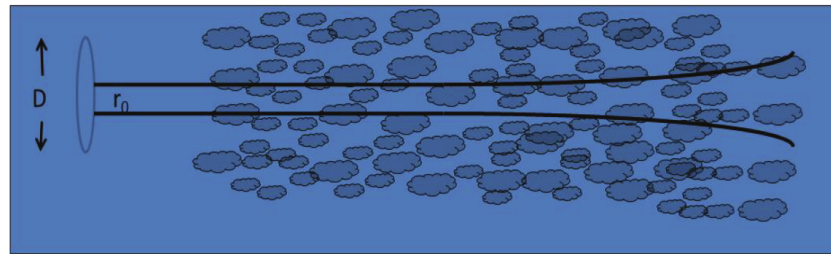


Figure 5.3: A representation of a beam transmitting through atmospheric turbulence

5.6 Speckle

When you illuminate an object with a narrowband laser beam, you see light and dark areas, which are called speckle. Speckle is interference that occurs due to scattering from one part of an object interfering with scattering from another part of the object (Figure 5.4).

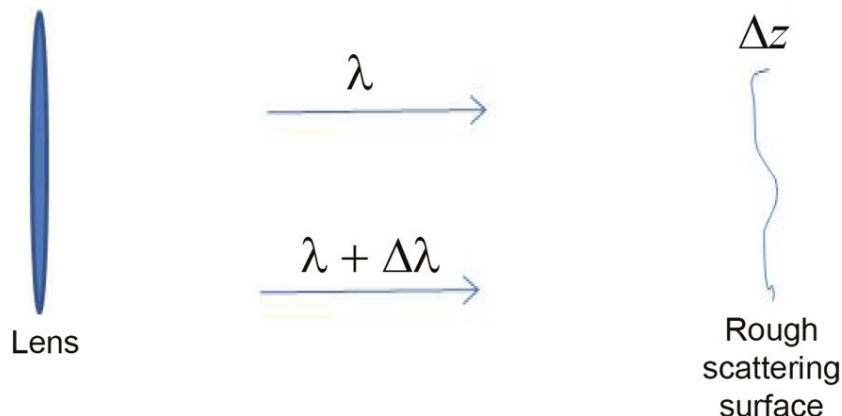


Figure 5.4: The effect of surface roughness on speckle

We do not see speckle when sunlight illuminates an object because there are many different wavelengths in the illuminating light, and the interference

from each wavelength averages out when added to all of the other wavelengths. If we use a laser with a broad spectral band, we can eliminate speckle in a direct-detection laser for the same reason that sunlight does not have speckle.

6 Types of LiDAR

LiDAR has a large number of available phenomenologies. There are therefore many types of LiDAR.

6.1 Direct-Detection LiDAR

1D, 2D, or 3D LiDAR can also be made in a coherent embodiment, but these LiDAR types usually use direct detection because phase information is not needed for these LiDAR modalities.

6.1.1 1D Range-Only LiDAR

A 1D image is a range profile of an object, with the only dimension being range. The range profile does not depend on the size of the receiving optical apertures, except for signal-to-noise considerations, so it can be used at long range if sufficient signal is available. This can be very useful in environments that are not cluttered and for objects that are far away, where the transverse dimensions of the object are not resolved by an optical system. A range profile gives the size of an object in one dimension and the distribution of its scattering centers along the orientation of that particular range profile.

6.1.2 Tomographic Imaging LiDAR

If we have multiple high-range-resolution 1D images from different directions, we can develop cross-range information as well as range information. The wider the angular distribution of the high-range-resolution images the better the cross-range imaging information. This is similar, but opposite, to the idea of stereo vision, where angle resolution is measured, but range information is inferred. In tomographic imaging, range information is measured from multiple angles, making it possible to infer cross-range information in the plane of the angle measurements. Figure 6.1 shows an airplane being viewed

from multiple angular locations. This type of angular diversity can be used to develop a range/cross-range image.

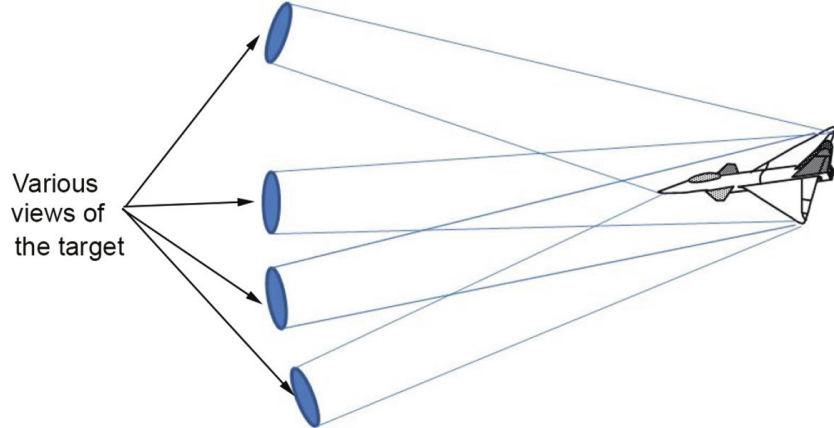


Figure 6.1: Multiple range-only images create a 2D image

6.1.3 Range-Gated Active Imaging (2D LiDAR)

Range-gated active imaging (2D LiDAR) is similar to passive imaging, but with illumination. The view is similar to what is generated by the eye, which also is a 2D sensor. For active gated imagers, the receiver is only open when the gate is open, so noise can only enter during that period. Active gated imagers increase SNR by decreasing the noise allowed into the receiver. One benefit of 2D LiDAR compared to passive sensing is that the camera can see at night while using a shorter-wavelength sensor.

6.1.4 3D Scanning LiDAR

Scanned LiDAR is one approach for collecting 3D images. This used to be the main approach until 2D high-bandwidth detector arrays became available. . A single detector, or a limited number of individual detectors, is scanned at a rapid rate to make a 3D image. Each detector has a sufficiently high bandwidth to measure the time of the return laser pulse accurately enough to provide range information to the precision desired. The need for a high-bandwidth detector response and readout in 3D imaging is the reason that scanning LiDAR has been popular, especially for commercial applications where cost is a significant issue.

A couple of significant, current, scanning LiDAR applications are 3D mapping and driverless cars, which are two of the largest applications of commercial LiDAR.

Figure ?? shows one implementation of a scanning LiDAR, in which a limited number of detectors are scanned in azimuth and then dropped down in elevation and scanned again.

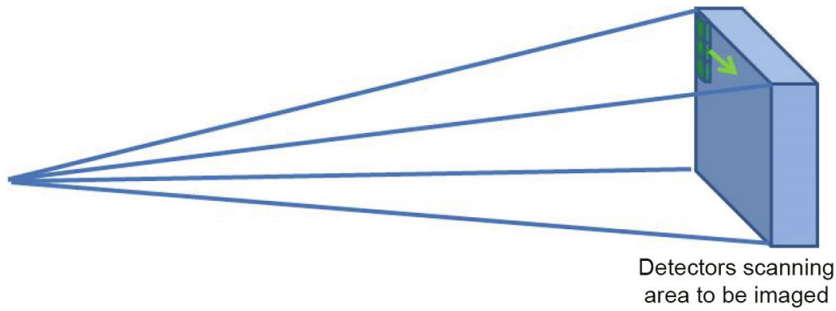


Figure 6.2: Scanning LiDAR representation

6.1.5 3D Flash Imaging

Flash imagers use a large array of detectors (e.g., a 128 x 128 pixel array) to develop the image. One of the first methods of large-array flash imaging used polarization change to measure range. This was done because at the time FPAAs with large format were not available with high-bandwidth detectors. More recently, high-bandwidth FPAs with appropriate ROICs have been developed. For flash imaging, the return laser power is imaged onto an array of detectors; therefore, we do not need to scan as fast, saving size, weight, and power. Also, for flash imagers, we only have to stabilize to a fraction of the angular size of the array, rather than to a fraction of the size of one DAS.

6.1.6 3D Mapping Applications

3D mapping systems have three variants: linear-mode scanning LiDAR, Geiger-mode LiDAR (GML), and single-photon LiDAR (SPL). Efficient 3D mapping requires careful consideration of various factors affecting the data collection and quality of data. This includes the local topography, vegetation, scene content, data accuracy requirements, spatial data reference information, desired acquisition window, weather conditions, unique conditions/restrictions, ground survey data acquisition, flight plans, tiling scheme, output

products, and application of rigorous quality control measures throughout the process. Mission, flight, and ground control plans are typically generated to support LiDAR data acquisition, and some of the collection parameters are used as metadata for processing the acquired raw data. Quality checks need to be performed preflight, inflight, and postflight to ensure that collected data pass quality requirements [i.e., no voids, cloud obstructions, shadows, or edge mismatch; point precision; and quality of data (e.g. precision dilution of precision (DOP) of the Global Positioning System (GPS) / Global Navigation Satellite System (GNSS)].

6.1.7 Laser Vibration Detection

The Doppler shift is used to measure velocity. It can provide a very accurate measure of velocity and as a result is often used to measure the small back-and-forth velocity caused by vibration. For vibration, we see a frequency-modulated return signal, with the frequency of the modulation as the vibration frequency and the magnitude of the frequency shifts equal to the varying Doppler shifts. The following equation shows the variation in position resulting from a vibration:

$$x = A \sin 2\pi ft \quad (12)$$

where A is the amplitude of the vibration and f is the frequency.

7 LiDAR Sources

Active EO sensors employ coherent sources in the wavelength region from the LWIR (around 10 mm) to the atmospheric transmission limit for UV light (around 200 nm). The sources can be based either on lasers or on nonlinear optical systems driven by lasers. Lasers are typically categorized by the type and format of the medium used to generate their output, which at the highest level are gases, liquids, and solids. Solid state lasers employ insulating solids (crystals, ceramics, or glasses) with elements added (dopants) that provide the energy levels needed for laser action. Energy to excite the levels is provided by other sources of light, either conventional sources such as arc lamps, or other lasers, in a process called optical pumping. Solid state lasers in turn are divided into two broad categories, bulk or fiber, with the

latter having recently emerged as an important technology for generation of high average powers with high beam quality, as discussed below. Even though they are also made from solid state materials, semiconductor lasers are considered as a separate laser category. While the lasers can be made to operate by optical pumping, if the semiconductor material can be fabricated in the form of an appropriate p–n junction, it is possible to pass electrical current through the junction and generate laser output directly. These diode lasers are by far the most widely used form of semiconductor laser and have led to major advances in source technology for active EO sensors.

Lasers of current interest for LiDARs are primarily diode lasers, fiber lasers, and bulk solid state lasers.

7.1 Laser Waveforms

Some fundamental laser issues are encountered when developing a LiDAR waveform. Direct-detection LiDARs cannot measure phase. They measure time of flight for range measurement by using pulses. When using a pulsed waveform, there is an advantage to using a laser capable of being Q switched if significant LiDAR range is desired.

Q-switching, sometimes known as giant pulse formation or Q-spoiling, is a technique by which a laser can be made to produce a pulsed output beam. The technique allows the production of light pulses with extremely high (gigawatt) peak power, much higher than would be produced by the same laser if it were operating in a continuous wave (constant output) mode.

With a Q-switched laser, it is possible to store a large amount of energy in the laser medium over a period of time and then release it all in a short pulse that is capable of accurately measuring range.

A limitation with pulsed lasers is the required range resolution. Short pulses allow better range resolution. Equation 3 gives range resolution as $\Delta R = c/2B$ where B is the bandwidth, and $1/B$ is the pulse width.

If we have a coherent LiDAR, we can use continuous-wave (cw) or high-duty-cycle waveforms. This can be done because range can be measured based on the changing frequency (or phase) of the laser, so we do not have to use pulsed lasers. For coherent LiDARs, however, a narrow-linewidth laser is required. If the laser is too broad in wavelength, it is impossible to measure phase by beating the return signal against the LO. Direct-detection LiDARs prefer short pulses, so a high-peak-power laser is required for long range. Coherent LiDARs need narrow-linewidth lasers. These are fundamental laser

parameters to consider when developing LiDARs. Most lasers now start with diode lasers as pumps because diode lasers are the cheapest and most efficient lasers. Diode lasers have problems both with high-power short pulses and with narrow linewidth. Neither of these issues is significant when using diode lasers to pump other lasers, but both can be significant when directly using diode lasers for LiDARs, especially long-range LiDARs. To accurately measure range, we need a high-bandwidth waveform that determines the range resolution (Equation 3). We need to be able to determine how long it took for light to travel from the LiDAR transmit aperture to the target and back to the LiDAR receive aperture. To accurately measure velocity using a coherent LiDAR, we need to measure the change in frequency due to Doppler shift. Measuring low frequencies requires a long measurement period. The simplest measurement period we can use for understanding LiDAR waveform is a single pulse.

As a rule of thumb, the speed of light is 0.3 m (or 1 ft) per ns. A laser pulse goes to the target and returns, so a 1-ns pulse will provide 0.15-m range resolution, or about 6 in. Range resolution is more precisely limited by the convolution of the pulse shape and the target, so pulse rise time can be a factor as well as pulse length. The range profile of the target gets into the calculation as well. For a coherent LiDAR we can measure velocity on a single pulse by using the Doppler shift:

$$\boxed{\Delta V = \frac{\lambda * \Delta f}{2}} \quad (13)$$

where ΔV is the velocity resolution, and Δf is the change in frequency due to the Doppler shift. The smallest Δf we can measure is one over twice the time of the measurement, so a difficulty with a short pulse that provides high range resolution is that you cannot measure velocity accurately. A 1-ns pulse would allow measurement of 1-GHz Δf , which for a l of 1.5 mm would measure velocity down to 750 m/s. To measure high range resolution and high velocity resolution, we can use a pulse doublet (Figure 7.1) or another high time– bandwidth product waveform. We use a single pulse width to accurately measure range, and a pulse train to measure Doppler shift and therefore velocity. The minimum number of pulses in a pulse train is a doublet. This is sometimes called a polypulse waveform if sampling requires more than two pulses.

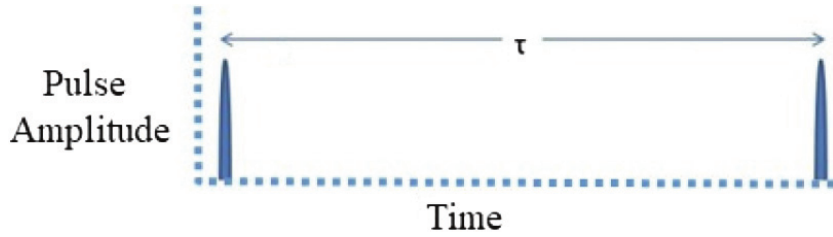


Figure 7.1: Pulse doublet waveform

7.1.1 High Time-Bandwidth Product Waveforms

An ideal coherent LiDAR waveform will allow precise measurement of both range and velocity with a single waveform. This is called a high time–bandwidth product waveform. For example, we could have two 1-ns pulses separated by 10 ms, providing 0.15-m range resolution and 7.5-cm/s velocity resolution for 1.5-mm light. This is referred to as having a time–bandwidth product of 10,000 because we have increased our velocity measurement capability by a factor of 10,000 while keeping the same range resolution.

7.1.2 Polypulse Waveform

A simple pulse doublet can be used (see Fig. 5.3) with the width of one pulse being used for range precision; however, the width between the front of the first pulse and the back of the last pulse can be used for velocity measurement resolution. The phase measured in the first pulse must be related to the phase measured in the second pulse. The laser must have a coherence time that equals or exceeds the time separation of the pulses. The coherence time is the period of time over which the phase of the signal is correlated between the phase at the beginning and the end of the coherence time. It is calculated as one over the linewidth B of the laser. The coherence length is the coherence time multiplied by the speed of light.

7.1.3 Linear Frequency Modulation

Range resolution is inversely proportional to the total signal bandwidth B (Equation 3).

7.1.4 Q-Switched Lasers for LiDAR

A laser with a long upper-state lifetime can build up energy in a cavity with no release. Then, suddenly, the Q of the cavity can be changed, switching out the stored energy in a single pulse. This pulse can be nanoseconds long, but can contain substantial amounts of energy, resulting in high peak power. This method is called Q switching because we are switching the Q of the cavity to release the energy stored in the laser medium. Q switching is a great way to efficiently generate high-energy nanosecond pulses. One method of Q switching is shown in Figure ???. A Pockels cell can be used to switch from almost no output from the cavity during a round trip to almost all of the energy being suddenly dumped out of the cavity.

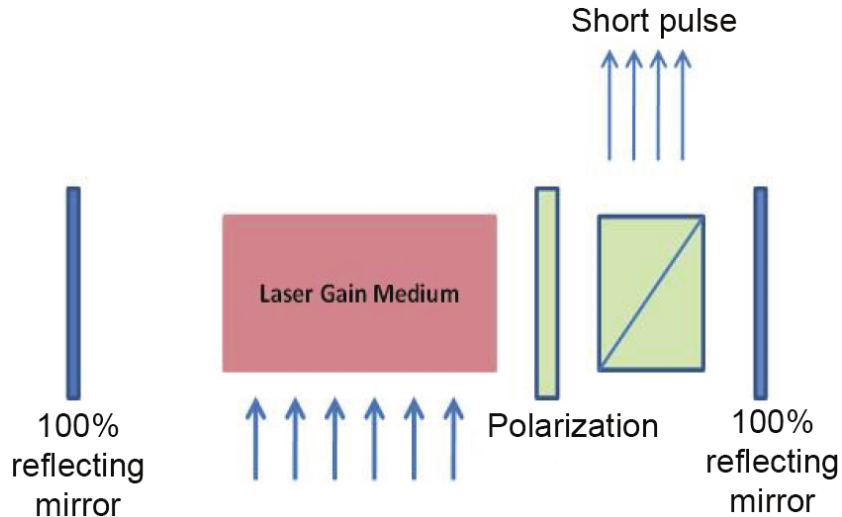


Figure 7.2: Geometry of an actively Q-switched laser using a Pockels cell

7.1.5 Diode Lasers of LiDARs

Diode lasers are used in almost all LiDARs today. In most cases, diode lasers are used as pumps for solid state lasers. In some cases, the diode lasers are used directly as emitters for the LiDAR. Diodes have the highest wall plug efficiency of any laser. Of course, this is expected since in most cases the other laser types start with a diode laser pump; therefore, any loss makes other laser types less efficient. Most diode lasers used for LiDAR are interband lasers, which use transitions from one electronic band to another.

8 LiDAR Receivers

8.1 Introduction

A good way to calculate LiDAR range is to use the equations in Chapter 5 to calculate how many photons are received in each detector given a certain emitted laser power, a certain aperture diameter, certain atmospheric conditions, etc. In this chapter, we calculate how many photons are required to detect a target in that detector, or pixel.

The purpose of a LiDAR receiver is to convert photons returned from the target into information. The type of LiDAR and its associated processing determine the exact information sought by the receiver. All LiDAR receiver types need to compete against noise. Much of this chapter will therefore cover approaches to extract signal in the presence of noise. By amplifying the returned signal, we can increase the signal-to-noise ratio (SNR). Signal-related noises such as background noise will be amplified, so amplification does not increase SNR with respect to those noises; however, it does help with certain noises, such as surface dark current noise because most of such noise is not amplified.

A very common approach to discriminate against this class of noises is to have gain in the receiver that amplifies the photocurrent generated by the signal. If we amplify the returned signal, additional noise, called excess noise, is introduced during the amplification process, but overall SNR is usually improved. We have two common forms of amplified, direct-detection LiDAR receivers: linear-mode avalanche photodiodes (LMAPDs) and Geiger-mode avalanche photodiodes (GMAPDs). LMAPDs linearly amplify the number of electrons generated, or the current, as the name indicates. GMAPDs always amplify the number of electrons to some large, maximum signal level.

To accurately measure range, we need a high-bandwidth detector or some equivalent high-bandwidth timing device because we measure range by measuring the time of flight of light to the target and return. This is one of the major differences between a LiDAR detector and a passive detector. Measuring range is important for 3D LiDAR. The higher the bandwidth of the detector the more precise the range measurements if there is a matching laser waveform unless something is done to make the bandwidth of the LiDAR effectively higher.

8.2 LiDAR Signal-to-Noise Ratio

We have to address how much energy per waveform is required for detection. To have detection, we need a certain SNR:

$$SNR = \frac{\langle i_s^2 \rangle}{\langle i_n^2 \rangle} \quad (14)$$

where i_s is the signal current and i_n is the mean noise current. We need to have a ratio of the mean squared signal current to the mean squared noise current that equals some threshold value. The mean squared signal current is :

$$\langle i_s^2 \rangle = G^2 \Re^2 P_s^2 \quad (15)$$

for detect detection, and :

$$\langle i_s^2 \rangle = 2n_h G^2 \Re^2 P_{LO} P_s \quad (16)$$

for coherent, or heterodyne, detection, where G is the preamplifier gain, \Re is the detector responsivity, P_s is the signal power, P_{LO} is the LO power, and n_h is the heterodyne mixing efficiency. We can further define the detector responsivity as :

$$\Re = \frac{n_q e}{h\nu} \quad (17)$$

where n_q is the detector quantum efficiency, e is the charge on an electron, h is Plank's constant, and ν is the carrier frequency of the light. Noise is denoted as :

$$\langle i_n^2 \rangle = \langle i_{shot,sig}^2 \rangle + \langle i_{shotLO}^2 \rangle + \langle i_{bk}^2 \rangle + \langle i_{dk}^2 \rangle + \langle i_{th}^2 \rangle \quad (18)$$

where i_{bk} is the shot noise on the background current, i_{dk} is the shot noise on the dark current, and i_{th} is thermal noise current. We separate signal and

LO shot noise terms because direct detection will not have LO shot noise. Received optical power converts to current, which has to be squared for direct detection to calculate the power term used in the SNR equation. The received optical power is related to the rate of arrival of the received photons by :

$$P_s = \frac{Nhc}{\lambda T_m} \quad (19)$$

where T_m is the period of time over which the measurement is made, and N is the number of photons per pixel received during that measurement time. So the SNR :

$$SNR = \frac{\langle i_s^2 \rangle}{\langle i_n^2 \rangle} = \frac{\langle i_s^2 \rangle = G^2 \Re^2 P_s^2}{\langle i_{shot,sig}^2 \rangle + \langle i_{shotLO}^2 \rangle + \langle i_{bk}^2 \rangle + \langle i_{dk}^2 \rangle + \langle i_{th}^2 \rangle} \quad (20)$$

8.3 Noise Probability Density Functions

The Noise probability density functions are discussed in detail on Chapter 6.2.1 of Paul McManamon - LiDAR technologies and systems [37].

8.3.1 Thermal Noise

Thermal noise, also known as Johnson or Nyquist noise, is electronic noise generated by the thermal agitation of charge carriers (usually the electrons) inside an electrical conductor. This noise occurs regardless of applied voltage. The energy from thermal noise is given by :

$$E_{th} = kTB \quad (21)$$

where k is Boltzmann's constant, T is temperature in Kelvin and is often assumed to be 300 K, and B is the bandwidth of the detector. Higher temperature creates more thermal noise. The current resulting from thermal noise is given by :

$$\boxed{\langle i_{th}^2 \rangle = \frac{4kTB}{R_L}} \quad (22)$$

where R_L is the load resistance. Thermal noise is not amplified by preamplifier gain, so it is one of the noises that is mitigated by having gain. Thermal fluctuations occur at all temperatures above absolute zero. Thermal noise is less important in LiDAR because the photons here contain more energy compared to radar, promoting the importance of a competing noise called shot noise. For 263 K shot noise is about $1/30_{th}$ of a photon in energy, with a wavelength of 1550 nm. Thermal noise is distinct from shot noise, which consists of additional current fluctuations that occur when a voltage is applied and a macroscopic current starts to flow.

8.3.2 Shot Noise

Shot noise is due to the quantization of an electromagnetic wave. Short wavelengths (high frequencies) have more energy per photon because :

$$\boxed{E_P = h\nu} \quad (23)$$

is the energy in a photon. In optics we use wavelengths more often than frequencies, so we rephrase Equation 23 as :

$$\boxed{E_P = \frac{hc}{\lambda}} \quad (24)$$

The quantization phenomenon occurs for microwave frequencies, but a joule of energy has many more photons at microwave frequencies. At a wavelength of $1.5\mu m$, a single photon has $1.3 \times 10^{-19} J$ versus $6.6 \times 10^{-24} J$ at 10 GHz (3-cm wavelength). There is a small variation in the arrival rate of photons. This variation provides a noise we call shot noise. Shot noise is a Poisson-distributed noise.

Shot noise in actual observations becomes indistinguishable from Gaussian noise except when the elementary events (photons, electrons, etc.) are so few that they are individually observed. Since the standard deviation of

shot noise equals the square root of the average number of events M, the SNR is given by :

$$SNR = \frac{M}{\sqrt{M}} = \sqrt{M} \quad (25)$$

Thus, when M is very large, the SNR is very large as well, and any relative fluctuations in M due to other sources are more likely to dominate over shot noise. The shot noise due to the signal return is :

$$\langle i_{shot,sig}^2 \rangle = 2eG^2F\Re P_S B \quad (26)$$

where F is the excess noise factor associated with the preamplifier gain. Excess noise is the noise added during the signal amplification process.

8.3.3 Background Noise

Background noise is just like signal, but it is signal we do not want. Since it is a form of signal, it will be amplified in the same manner as signal when we use amplification to discriminate against some noise sources. The sun is often a strong source of background noise, so we will calculate its impact. In the visible range, the sun is a strong background noise. Often we can reduce background noise by using a narrowband filter and a narrowband laser.

Commercially available narrowband filters can be placed in the receiver optical path to block unwanted background light. We assume that the narrowest achievable bandwidth at a reasonable cost is approximately $\sigma_{min} - 1nm$ for collimated (to make (light rays, etc.) parallel. 2. to adjust the line of sight of (a telescope, surveyor's level, etc.)) light at normal incidence.

8.3.4 Dark Current Noise

Dark current noise is the noise in a detector when that detector is not illuminated by any light. The charge generation rate in a detector can be related to specific crystal defects within the depletion region of a detector (bulk defects). Bulk dark current participates in preamplifier gain. Bulk defects are

the most likely sources of dark current. Surface defects can also contribute to dark current but are much less likely to be a source compared to bulk defects. Surface dark current does not participate in preamplifier gain. Both bulk- and surface-generated dark current primary carriers are Poisson distributed. The pattern of different dark currents can result in a fixed-pattern noise. Dark frame subtraction can remove an estimate of the mean fixed pattern, but a temporal noise still remains because the dark current itself has a shot noise. Dark current is not noise. It is unwanted signal. Like any signal, it contains noise. The noise from dark current is calculated as :

$$\langle i_{dk}^2 \rangle = 2eB(I_{dks} + I_{dkb}G^2F) \quad (27)$$

where I_{dks} is surface dark current that is not multiplied in an APD, and I_{dkb} is bulk dark current that is multiplied by the gain of an APD. When you amplify a signal, you add additional noise, which is denoted by the excess noise factor F.

8.3.5 Avalanche Photodiodes

One way to reduce the effects of noise on a LiDAR is to employ gain either before the detector, or in the detector. We could use a fiber preamplifier, which would amplify the signal prior to it hitting a detector. The avalanche photodiode (APD) is the solid state equivalent of the photo- multiplier tube in that both create many electrons from each incident photon. The number of electrons created per absorbed photon is the internal detector gain. The noise associated with the gain process is called excess noise. The gain directly improves the SNR in situations where system noise, such as dark current, limits the performance.

We discuss two classes of APDs as LiDAR detectors: LMAPDs GMAPDs. LMAPDs are operated below their breakdown voltage, generating current pulses that are on average proportional to the strength of the optical signal pulse. LMAPDs normally operate with high-gain current, or charge amplifiers, which develop an output voltage waveform that is proportional to the LMAPD's photocurrent waveform. In contrast, GMAPDs are armed by biasing them above their breakdown voltage, rendering them sensitive to single primary charge carriers.

As part of the discussion on APDs, we use a single scenario to judge the amount of energy required to make a 3D map of a given area. The

scenario chosen uses a large DAS because that creates more issues that must be addressed due to the large background radiation from the sun. As stated earlier, one way to reduce the effect of noise in direct detection is to use gain. Expanding the noise terms, we have :

$$SNR = \frac{G^2 \Re^2 P_s^2}{2eBG^2F\Re[P_S + P_{bk} + P_{dkb}] + 2eBi_{dks} + 4ktB/R_L} \quad (28)$$

Gain after detection will reduce the influence of surface dark current and thermal noise. Background radiation will be amplified by the same amount as the signal. Bulk dark current will also be amplified in an APD; amplification will add noise. For background-limited direct detection, we have :

$$SNR = \frac{n_D P_s^2}{2hvBF P_{dkb}} \quad (29)$$

where n_D is the detector quantum efficiency, and we have made use of the fact that :

$$\Re = \frac{n_D e}{hv} \quad (30)$$

In the limit where the signal shot noise dominates the other noise terms, the SNR is given by

$$SNR_{shotlim} = \frac{n_D P_S}{2hvBF} \quad (31)$$

Within the limit where the signal shot noise dominates other noise terms, the SNR is directly proportional to the number of photons received. This is the best we can do and is the goal of using gain.

9 LiDAR

9.1 Coherent LiDAR

Coherent LiDARs can also measure phase by beating the return signal against the LO in contrast with direct-detection LiDAR sensors.

10 Lane Detection

Lane detection plays a vital role in autonomous driving. Reliable lane detection can help autonomous driving systems to make the also decisionsh. Lane detection algorithms get to be a challenging task due to many factors such as the wide variety of lane markings, the complex and changeable road conditions, and the inherent slender features of lane markings. To accomplish traditional lane detection computer vision techniques are used e.g. Canny Edge Detection.

In this project, row detection with deep learning will be used to determine the position of the legged robot while moving through vineyards. Deep learning needs a dataset for training and a dataset for testing, and because row detection with vineyards as lanes is not common these datasets have to be created by us.

11 Visual Odometry (VO)

In robotics and computer vision, visual odometry is the process of determining the position and orientation of a robot by analyzing the associated camera images. Visual Odometry methods can be divided into 2 sub-categories [39]:

- Geometric Approaches : Exploit information from the projective geometry.
 - Feature-Based : The feature-based techniques extract distinct interest points that can be tracked with the help of vectors describing the local region around the key-points. These techniques are dependent on the image texture and are generally not applicable in texture-less or low texture environments such as sandy soil, asphalt, etc.

- Appearance-Based : The appearance-based techniques operate on intensity values directly and matches template of sub-images over two frame or the optical flow values to estimate motion.
- Non-Geometric Approaches : Are based on learning.
 - Learning-Based : The learning based VO scheme trains regression model to estimate motion parameter when fed with labeled data.

There are additionally hybrid approaches that utilize 2 or even all of the above techniques. For example, Scaramuzza Siegwart proposes a hybrid of appearance and feature based approach, a combination of visual camera and LIDAR sensor, vision and IMU, vision and compass, etc [40].

11.1 Feature-Based Approach

This scheme matches distinct feature between stereo images and triangulates them to the 3-D world frame. Once the robot moves, these feature points are matched in the next frame to obtain corresponding 3D point and generate motion parameters.

12 Ideas

- Using the wheel rotation to calculate distance travelled, to reduce errors on localization
- Use 2 zed cameras one on head one on belly pointing the same way (distance known from each other), after feature matching on both compare the save features to have an even more accurate position of the point-cloud

List of Figures

2.1	RTK Base and Rover	7
2.2	RTK Base and Multiple Receivers	8
2.3	How NTRIP Works	9
2.4	Ellipse Series Product Line	11
2.5	Mechanical Properties of the Product Line	12
2.6	Accuracy and Interfaces	13
2.7	Sensor Properties	14
2.8	Pressure Sensor Properties	14
2.9	Electrical and Environmental Properties	15
2.10	AsteRx SBi3 Pro+	16
2.11	Mti-680G's Sensor fusion Performance and Sensing Components	17
2.12	Mti-680G's System Specifications	17
2.13	Mti-680G	18
2.14	X1 Specifications	19
2.15	X1 GNSS/INS Receiver	19
2.16	μ INS	21
2.17	3DMGQ7 GNSS/INS Specifications	22
2.18	3DMGQ7 GNSS/INS	22
3.1	How Solid State LiDAR Works	24
3.2	Solid State LiDAR Detection	25
3.3	Velarray H800	26
3.4	Velarray M1600	27
3.5	Velabit	28
3.6	RS-LiDAR-M1	29
3.7	RS-LiDAR-M1 Specifications	30
3.8	S3-2	31
3.9	S3-2 Specifications	32
3.10	Cube 1 Specifications	33
3.11	Cube 1	33
3.12	Cube Range 1 Specifications	34
3.13	Cube Range 1	35
3.14	L515 Specifications	36
3.15	L515	37
3.16	4Sight	38
3.17	4Sight Specifications	38
3.18	OS0, OS1, OS2 Differences and Specifications	39

3.19 OS0, OS1 and OS2 (Left to Right respectively)	40
3.20 HSP-3D160 Pro	41
3.21 HSP-3D640	41
3.22 HSP-3D160 vs HSP-3D640	42
3.23 Leddar Pixell	43
3.24 Leddar Pixell's Specifications	43
3.25 Avia	44
3.26 CE30	45
3.27 Aeries I	46
3.28 Aeries I's Key Features	46
3.29 Aeries II	46
3.30 Aeries II's Key Features	47
3.31 Iris	47
3.32 Sora Family	48
3.33 Sora-P60 Specifications	49
3.34 Sora-P90 Specifications	49
3.35 Vista-X90	50
3.36 Vista-X120	50
3.37 Vista-X90 Specifications	50
3.38 Vista-X120 Specifications	50
3.39 Nova	51
3.40 Nova Specifications	51
3.41 QT128	52
3.42 QT128 Specifications	53
3.43 AT128	54
3.44 AT128 Specifications	54
3.45 Pandar128	55
3.46 Pandar128 Specifications	55
3.47 XT32	56
3.48 XT32 Specifications	57
3.49 POWER-W	58
3.50 POWER-PBA2	58
3.51 ULTRA-UGC1	59
3.52 ULTRA-UGC2	60
3.53 TetraVue 4D Flash LiDAR	60
3.54 AX32	61
3.55 AX32 Specifications	62
3.56 OPAL-3 Conical	63

3.57	OPAL-3 Panoramic	63
3.58	InnovizOne	64
3.59	InnovizTwo	65
3.60	Innoviz360	66
3.61	InnovizPro	66
3.62	Lumotive M30	67
3.63	Lumotive U30	67
3.64	Lumotive L30	68
3.65	ML	69
3.66	ML Specifications	69
3.67	XenoLidar Xact	70
3.68	SP2.5	70
3.69	SP3.0	71
3.70	Spectrum HD	71
3.71	Spectrum Off-Road	72
3.72	ibeoNEXT	72
3.73	ibeoLUX	73
3.74	ibeoLUX Specifications	74
3.75	A-Sample LiDAR	75
4.1	LiDAR Conceptual Diagram	80
4.2	LiDAR Sampling Possibilities	82
4.3	Transmit/Receive Isolation Using Polarization	84
5.1	The shape of (left) a Gaussian beam compared to a super-Gaussian beam (right) with $N = 5$	85
5.2	Clipped Gaussian beam with $c = 1$ and aperture diameter = 2.5 .	86
5.3	A representation of a beam transmitting through atmospheric turbulence	88
5.4	The effect of surface roughness on speckle	88
6.1	Multiple range-only images create a 2D image	90
6.2	Scanning LiDAR representation	91
7.1	Pulse doublet waveform	95
7.2	Geometry of an actively Q-switched laser using a Pockels cell .	96

References

- [1] RTK GPS, Wiki.
- [2] Ellipse-D SBG Systems, SBG Systems Site.
- [3] AsteRx SBi3 Pro+, Septentrio, Septentrio Site.
- [4] MTi-680G XSens, XSENS Site.
- [5] X1 BYNAV, BYNAV Site.
- [6] μ INS Intertial Sense, Intertial Sense Site.
- [7] 3DMGQ7-GNSS/INS Parker Lord, Parker Lord Site.
- [8] Velarray H800 Velodyne, Velodyne Site.
- [9] Velarray M1600 Velodyne, Velodyne Site.
- [10] Velabit Velodyne, Velodyne Site.
- [11] RS-LiDAR-M1 Robosense, Robosense Site.
- [12] S3-2 Quanergy, Quanergy Site.
- [13] Cube 1 Blickfeld, Blickfeld Site.
- [14] L515 Intel, Intel Realsense Site.
- [15] 4SIGHT M AEYE, AEYE Site.
- [16] Hypersen, Hypersen Site.
- [17] Leddar Pixell LeddarTech, LeddarTech Site.
- [18] AVIA Livox, Livox Site.
- [19] Aeries AEVA, AEVA Site.
- [20] Iris Luminar, Luminar Site.
- [21] Sora-P Family Cepton, Cepton Site.
- [22] Vista-X Family Cepton, Cepton Site.

- [23] Nova Cepton, Cepton Site.
- [24] Hesai, Hesai Site.
- [25] Genius-Pros, Genius-Pros Site.
- [26] 4D Flash LiDAR tetravue, tetravue Site.
- [27] AX3010 ABAX SENSING, ABAX SENSING Site.
- [28] OPAL-3 Canonical/Panoramic, NeptecTechnologies Site.
- [29] Innoviz, Innoviz Site.
- [30] Lumotive, Lumotive Site.
- [31] ML SosLab, SosLab Site.
- [32] Xenomatix, Xenomatix Site.
- [33] Opsys, Opsys Site.
- [34] Baraja, Baraja Site.
- [35] Ibeoautomotive, Ibeoautomotive Site.
- [36] A-Sample Microvision, Microvision Site.
- [37] Paul McManamon (2019) *LiDAR Technologies and Systems*
- [38] Visual Odometry, Wikipedia Site.
- [39] Poddar, Shashi Kottath, Rahul Karar, Vinod. (2018). Evolution of Visual Odometry Techniques.
- [40] D. Scaramuzza and R. Siegwart, "Appearance-guided monocular omnidirectional visual odometry for outdoor ground vehicles," IEEE transactions on robotics, vol. 24, pp. 1015-1026, 2008.